Check for updates

Design Principles and Mechanistic Understandings of Non-Noble-Metal Bifunctional Electrocatalysts for Zinc–Air Batteries

Yunnan Gao[1], Ling Liu[1], Yi Jiang[1] ✉, Dexin Yu[1], Xiaomei Zheng[4], Jiayi Wang[3], Jingwei Liu[1], Dan Luo[1], Yongguang Zhang[1] ✉, Zhenjia Shi[1], Xin Wang[3], Ya-Ping Deng[2] ✉, Zhongwei Chen[1] ✉

HIGHLIGHTS

- The recent advances in non-noble-metal bifunctional electrocatalysts for zinc–air batteries are summarized with the design principles.

- The working mechanism are discussed to provide a comprehensive understanding of the structure-performance relationship of electrocatalysts and the reaction pathways of the oxygen redox reactions.

- The challenges and prospects related to designing advanced non-noble-metal bifunctional electrocatalysts for high performance zinc–air batteries are provided.

ABSTRACT Zinc–air batteries (ZABs) are promising energy storage systems because of high theoretical energy density, safety, low cost, and abundance of zinc. However, the slow multi-step reaction of oxygen and heavy reliance on noble-metal catalysts hinder the practical applications of ZABs. Therefore, feasible and advanced non-noble-metal electrocatalysts for air cathodes need to be identified to promote the oxygen catalytic reaction. In this review, we initially introduced the advancement of ZABs in the past two decades and provided an overview of key developments in this field. Then, we discussed the working mechanism and the design of bifunctional electrocatalysts from the perspective of morphology design, crystal structure tuning, interface strategy, and atomic engineering. We also included theoretical studies, machine learning, and advanced characterization technologies to provide a comprehensive understanding of the structure-performance relationship of electrocatalysts and the reaction pathways of the oxygen redox reactions. Finally, we discussed the challenges and prospects related to designing advanced non-noble-metal bifunctional electrocatalysts for ZABs.

KEYWORDS Zinc–air batteries; Bifunctional electrocatalysts; Design principles; Mechanistic understandings

---
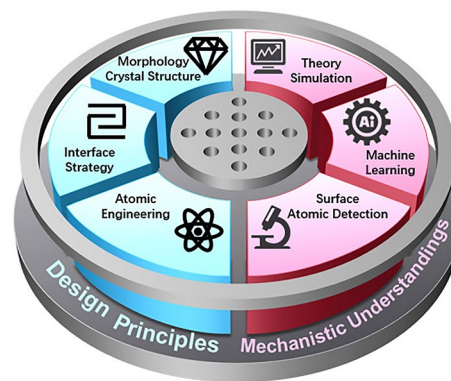
Yunnan Gao, Ling Liu and Yi Jiang have contributed equally to this work.

✉ Yi Jiang, jiangy0719@dicp.ac.cn; Yongguang Zhang, ygzhang@dicp.ac.cn; Ya-Ping Deng, ya-ping.deng@uwaterloo.ca; Zhongwei Chen, zwchen@dicp.ac.cn

[1] Power Battery and Systems Research Center, State Key Laboratory of Catalysis, Dalian Institute of Chemical Physics, Dalian Institute of Chemical Physics, Chinese Academy of Sciences, Dalian 116023, People's Republic of China

[2] Department of Chemical Engineering, University of Waterloo, Waterloo, ON N2L 3G1, Canada

[3] Institute of Carbon Neutrality, Zhejiang Wanli University, Ningbo 315100, People's Republic of China

[4] College of Materials and Chemistry, China Jiliang University, Hangzhou 310018, People's Republic of China

1 Introduction

The consumption of large quantities of fossil energy accompanied by high carbon dioxide emissions has led to an energy crisis and climate change. Electrochemical energy storage and conversion are important for reducing the use of fossil energy and promoting a green, renewable, and efficient living environment. In the past decades, the field of battery systems has progressed considerably [1]. Three generations of batteries, including lead-acid battery [2], Ni-MH battery [3] and lithium-ion battery [4–6] (LIBs), were designed and commercialized. Among them, LIBs have received the most attention from researchers and have been popularized in various areas ranging from portable electric devices to large power systems, especially electric vehicles (EVs). However, the low specific energy density of the currently available LIBs greatly constrains the driving range of EVs. LIBs not only have inferior performance that cannot satisfy the growing demand of the industry, but the highly active Li also causes some serious safety issues [7–10]. To resolve these problems, many researchers have investigated next-generation battery systems that have a higher energy density and are safer and cheaper. Although several battery types were proposed as possible replacements, such as Na-ion [11], K-ion [12], Na–S [13], and Li–S battery [14], all of them had certain shortcomings that greatly limited their feasibility. For example, Na-ion batteries have a considerably lower energy density and greater risk compared to the available Li-ion batteries [15–17]. Similarly, for Li–S batteries, further studies are still required to address their low electronic conductivity due to the presence of sulfur, large variation in their volume, and severe shuttle effects during cycling [18, 19]. Therefore, it is challenging for these technologies to meet the increasing demands demand for battery systems in the future. Thus, high-energy/power density, durable, and safe energy storage systems need to be developed.

Metal-air batteries (MABs) have received much attention from researchers and have been extensively studied due to their high theoretical energy density (about 800–8100 Wh kg^{-1}) that is several folds higher than that of LIBs (about 200–250 Wh kg^{-1}) and renewable fuel resources, as they are powered by oxygen in the air [20]. Some researchers have investigated several MABs, including Li–O_2 [21], Na–O_2 [22], K–O_2 [23], Zn–air [24], Mg–air [25], Al–air

[26] and Fe–air [27] batteries. Typically, MABs are of two types based on the different types of electrolytes used. One type is based on alkali anodes and uses aprotic electrolytes, including Li, Na, and K, which are usually known as O_2 batteries instead of MABs, as they use pure O_2 as the cathode fuel to minimize the negative effects of CO_2 and moisture on the anode [20]. The electrolyte used for Zn–air, Mg–air and Al–air is aqueous. Although researchers have used various strategies to make them practically feasible, three major concerns hinder their large-scale commercial application: (1) serious safety concerns regarding the high reactivity of these alkali anodes and flammable organic electrolytes; (2) high cost to meet the strict manufacturing criteria; (3) environmental pollution, such as metal/heavy metal-related, electrolyte contamination, air pollution, etc. [28, 29]. In contrast to alkali MABs, aqueous-based MABs have considerable advantages, including greater safety, decent conductivity, lower cost, and more eco-friendly. Thus, aqueous-based MABs have received much attention from researchers for further improving their electrochemical performance [30].

Although Mg–air and Al–air batteries have a very high theoretical energy density and discharge voltage, their poor rechargeability limits their commercial application. The problem occurs mainly because the electroreduction of Mg^{2+} and Al^{3+} in aqueous electrolyte is not feasible. Limitations in such primary battery configurations greatly decrease the practical values of the two batteries [31]. As Fe–air batteries are considerably cheaper than other systems, some rechargeable prototypes were developed, which showed cyclability of over 1000 cycles. However, the performance of iron electrodes is limited by the evolution of hydrogen and electrode passivation [32]. The company called Form Energy may solve the problems based on the "reversible oxidation of iron". The Fe–air batteries developed by Form Energy might scale up from a lab-scale prototype to a grid-scale plant, to provide 150 h of power at one-tenth of the cost of lithium batteries by 2025. Compared to the above-mentioned metal-air batteries (Table 1), Zn-air batteries (ZABs) are better MABs with a suitable theoretical energy density (1086 Wh kg^{-1}), non-toxicity, low cost (3.00 $ per kg Zn), and safety.

So far, some companies, such as EOS Energy Storage, Fluidic Energy, and ZincNyx Energy Solutions, have joined the investigation and contributed immensely to the research on ZABs, whereas the products are still at an early stage.

Table 1 Comparison of various metal air batteries

Battery type	Cell voltage (V)	Specific energy (Wh kg^{-1})	Cost ($ per kg)	Electrolyte	Rechargeable	Advantage	Disadvantage
Li–O$_2$	2.96	5930	185.1	Aprotic	Yes	High energy density	Unsafe operation, poor reversibility, poor cycle life
Na–O$_2$	2.3	1680	2.7	Aprotic	Yes		
K–O$_2$	2.37	1190	22.6	Aprotic	Yes		
Zn–air	1.65	1220	2.9	Aqueous	Yes	Suitable theoretical energy density, nontoxicity, low cost, safety	Lack of active and durable bifunction-al electrocatalysts on the cathode
Mg–air	3.09	5240	3.0	Aqueous	No	High theoretical energy density and discharge voltage	Poor rechargeability and practical values
Al–air	2.71	5780	2.6	Aqueous	No		
Fe–air	1.28	1080	0.5	Aqueous	Yes	Low cost, good cyclability	Evolution of hydrogen and electrode passivation

Some limitations of anodes need to be addressed, such as dendrite formation, shape change, passivation, corrosion, and side reactions with electrolytes (hydrogen evolution reaction) during cycling [33]. Many studies have investigated ways to enhance the cycling lifetime by incorporating Zn, using strategies primarily involving the introduction of additives to the anode, electrolyte, or separator to resolve various problems associated with the anode [34–36]. Oxygen electrocatalytic redox reactions, including oxygen reduction reactions (ORR) for discharging and oxygen evolution reactions (OER) for charging, are the cathode reactions that occur at the air electrode. The key barrier lies on the side of the cathode, i.e., the lack of active and durable bifunctional electrocatalysts, which has motivated many researchers to use various techniques to identify suitable candidates [37].

The benchmark electrocatalysts are mostly made from precious metal materials, i.e., Pt/C for ORR and RuO$_2$/IrO$_2$ for OER; however, their high cost and low abundance limit their practical application [38, 39]. Therefore, studies on efficient and cheap bifunctional electrocatalysts are necessary to promote further commercialization of ZABs, although the task is challenging. The non-noble-metal electrocatalysts, including transition metal compounds, carbon-supported transition metal materials, and metal-free carbon, exhibit promising electrolytic performance.

Some previous reviews have discussed rechargeable ZAB technology for each part to the configuration of the whole battery [40–42], nonetheless, few studies have explained the state-of-the-art design strategies of non-noble-metal bifunctional electrocatalysts for ZABs concerning structure-performance relationships. To establish a positive paradigm, here, we presented a review emphasizing the recent progress in bifunctional electrocatalysts for application in rechargeable ZABs. We also provided detailed information and guidance for future design and development. First, we discussed the progress of ZABs in the past two decades and provided an overview of the key developments in this field. Then, we highlighted the working principles and the design of the electrocatalysts based on morphology, crystal structure, interface, and atomic level. We combined theoretical studies and advanced/in situ characterization technologies to discuss the structure–function relationship of electrocatalysts and the reaction pathways of the oxygen redox reactions. Finally, we discussed the challenges to the development of bifunctional electrocatalysts and summarized research prospects.

2 History of Zinc–Air Batteries

Research on Zinc–air batteries started in 1866 when Georges-Lionel Leclanché developed the first ZABs using ammonium chloride solution [43]. Afterwards, Heise and Schumacher used an alkaline electrolyte, which exhibited a long duration of 12–18 months [44]. Although a high energy density of 200 Wh kg^{-1} for ZABs by virtue of the stack cell configuration, ZABs developed in a slow rate till the 1980s due to the increased research attention on H$_2$–O$_2$ fuel cells with advanced gas-diffusion electrodes. Then, the emergence of Li-ion batteries halted further research on

ZABs. However, Li-ion batteries have limitations such as a low theoretical energy density, severe safety hazards caused by organic electrolytes, harmful to the environment, and scarcity of resources [45]. Hence, the application of ZABs using an aqueous electrolyte was proposed again because of their advantages of safety and environmental friendliness. The iteration of advanced techniques and theoretical computation modeling were combined to develop a more efficient way to design ZABs. One promising direction of research involves the development of electrocatalysts that can facilitate ORR and OER, which are critical processes in many electrochemical energy devices. In 2012, Chen et al. published a study in which they fabricated a bifunctional electrocatalyst that could simultaneously catalyze the ORR and OER [46]. Their seminal study provided new insights into the catalyst design of cathode reactions. In 2013, Dai et al. developed a new electrocatalyst with a high energy density (700 W h kg^{-1}) [47]. After the development of bifunctional electrocatalysts for ORR and OER by Chen et al. and Dai et al., significant advancements were made in the design of efficient and durable catalysts for application in energy conversion and storage. Researchers have developed various strategies for improving the performance of bifunctional catalysts, including their morphology, structure, and atomic-level design. For example, Fu et al. implemented a strategy for developing bifunctional catalysts. They designed a durable and efficient three-dimensional bifunctional air electrode by building a hair-like Co_3O_4 nanowire array on a stainless steel mesh current collector [48]. The electrode developed exhibited superior performance for the ORR and OER; thus, they made a promising candidate for flexible energy storage applications. To understand the design principles of the catalyst for the cathode, Wu et al. used advanced characterization techniques and found that stable gas–solid-liquid triple-phase reaction areas synergistically optimized electron conduction, oxygen gas diffusion, and ion transport for electrocatalysis, which ultimately improved the performance of ZABs [49]. In 2021, Sun et al. used theoretical methods, such as density functional theory (DFT), to identify reaction mechanisms and processes at the molecular level. They designed an air cathode with a water-poor and zinc ion-rich inner Helmholtz layer, which facilitated stable operations in ambient air and good reversibility [50]. By systematically combining theory, experiment, characterization, and electrolyzer design, a new paradigm emerged, which promoted the practical application of ZABs. The development of zinc batteries as power batteries for electric vehicles can effectively reduce carbon emissions and further advance the transition to a future with cleaner energy. However, several challenges need to be addressed before zinc batteries can be used extensively for commercial purposes. These challenges include optimizing the performance of the battery, improving its durability, and reducing the cost of production to make it more commercially viable. Researchers have made significant progress in these areas, and thus, zinc batteries might play an important role in sustainable transportation in the future.

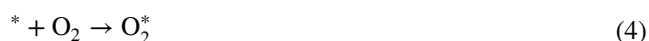# 3 Working Principles of the ZABs

3.1 Battery Reaction Mechanisms

There are several key components, including an aqueous electrolyte, a separator, a Zn anode, and an air cathode. In most cases, ZABs use a concentrated alkaline solution containing Zn salts, usually ZnO or $Zn(CH_3COO)_2$, to maintain the electrolyte with high oxygen diffusion coefficients and ionic conductivity at about 640 mS cm^{-1} (30 wt% KOH solution at 25 °C). For the Zn anode, metallic plates or powders are mostly applied and undergo a two-electron redox of Zn^{2+}/Zn couple during the discharge process (Eqs. 1 and 2). In contrast, $Zn(OH)_4^{2-}$ is reduced to metallic Zn by accepting electrons when charged [51].

$$Zn + 4OH^- \leftrightarrow Zn(OH)_4^{2-} + 2e^- \tag{1}$$

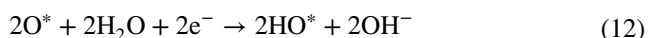$$Zn(OH)_4^{2-} \leftrightarrow ZnO + 2OH^- + H_2O \tag{2}$$
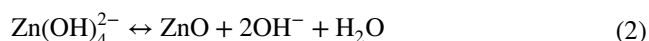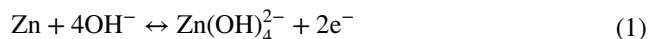
Electrocatalysts associated with air electrodes simultaneously catalyze ORR and OER during the operation of ZABs. The ORR branch is usually illustrated as the following procedure: the catalyst first contacts with the O_2 in the environment and adsorbs it at the active site, then the O–O bonds are broken, leading to the formation of oxygen intermediates, and finally, the produced OH$^-$ diffuses into the electrolyte [52]. These reaction steps are shown below (* represents the active site of the catalyst):
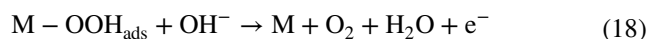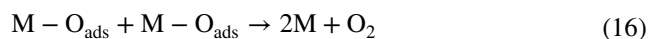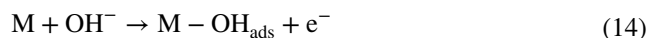
Bidentate O_2 adsorption:

$$O_2 + 2H_2O + 4e^- \rightarrow 4OH^- \tag{3}$$

$$^* + O_2 \rightarrow O_2^* \tag{4}$$

$$O_2^* + H_2O + e^- \rightarrow HOO^* + OH^- \tag{5}$$

$$HOO^* + e^- \rightarrow O^* + OH^- \tag{6}$$

$$O^* + e^- + H_2O \rightarrow OH^- + OH \tag{7}$$

$$OH^* + e^- \rightarrow OH^- + ^* \tag{8}$$

End-on O_2 adsorption:

$$O_2 + H_2O + 2e^- \rightarrow HO_2^- + OH^- \tag{9}$$

$$^* + O_2 \rightarrow O_2^* \tag{10}$$

$$O_2^* \rightarrow 2O^* \tag{11}$$

$$2O^* + 2H_2O + 2e^- \rightarrow 2HO^* + 2OH^- \tag{12}$$

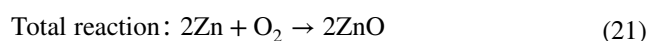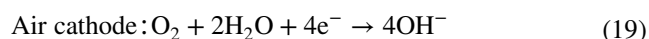$$2HO^* + 2e^- \rightarrow 2OH^- + ^* \tag{13}$$

An ORR may proceed along either a $4e^-$ route according to Eq. (3) or a $2e^-$ route as shown in Eq. (9). The specific reaction pathway depends on the configuration of the active sites in electrocatalysts. The adsorption of O_2 can occur in two ways: bidentate O_2 adsorption with two oxygen atoms coordinated with the electrocatalyst, and end-on O_2 adsorption, i.e., one oxygen atom coordinated perpendicularly to the catalyst. The former adsorption method primarily occurs via the $4e^-$ route with direct hydroxyl formation (as shown in Eqs. 4–8), while the latter one usually leads to a $2e^-$ route with peroxide production (as shown in Eqs. 10–13). The peroxides formed in the $2e^-$ route is corrosive, which can destroy the cycling stability. In practice, those electrocatalysts which can direct the ORR toward the $4e^-$ route are in high demands [53].

The OER is the reverse of ORR but with important differences in the design of the catalyst. Considering that the OER process has decent activity and stability, metal-based materials are used to illustrate the OER mechanism. The OER process in an alkaline electrolyte is shown in the equations below, where M represents the active site in the electrocatalysts and "ads" represents the adsorbed species at the active sites. The OER pathway begins with the coordination of hydroxyl ions at the active sites, as shown in Eq. (14), and then, several steps occur according to two routes. In one route (Eqs. 15 and 16), O_2 is produced by the coupling reaction between the two M–O_{ads} intermediates. Another route involves Eqs. (15)–(17) and (18), where M–OOH_{ads} is generated by reactions between M–O_{ads} and

OH. Then, M–OOH_{ads} further reacts with OH^- to form O_2. Theoretically, the reaction barrier of the former reaction route is higher [54].

$$M + OH^- \rightarrow M - OH_{ads} + e^- \tag{14}$$

$$M - OH_{ads} + OH^- \rightarrow M - O_{ads} + H_2O + e^- \tag{15}$$

$$M - O_{ads} + M - O_{ads} \rightarrow 2M + O_2 \tag{16}$$

$$M - O_{ads} + OH^- \rightarrow M - OOH_{ads} + e^- \tag{17}$$

$$M - OOH_{ads} + OH^- \rightarrow M + O_2 + H_2O + e^- \tag{18}$$

Although alkaline electrolytes are commonly used in ZABs, they are susceptible to zinc dendrite formation, ZnO precipitation, electrode corrosion, and electrolyte degradation, which can decrease cycle stability and battery life. To overcome these challenges and improve the performance of ZABs, neutral or near-neutral electrolytes are used. In a neutral medium, the reactions at the air cathode are the same as those in alkaline electrolytes, but the reactions at the zinc anode are different due to a significant decrease in the concentration of $Zn(OH)_4^{2-}$ caused by the absence of OH^-. This can be seen in Eqs. (19–21).

$$\text{Air cathode} : O_2 + 2H_2O + 4e^- \rightarrow 4OH^- \tag{19}$$

$$\text{Zinc anode} : Zn^{2+} + 2e^- \rightarrow Zn \tag{20}$$

$$\text{Total reaction} : 2Zn + O_2 \rightarrow 2ZnO \tag{21}$$

Many types of electrolytes have been developed, whereas alkaline electrolytes are the most commonly used because the catalysts in them are more stable and have higher activity [55]. As many studies are already available on electrolytes [56, 57], we have not discussed them in this study.

3.2 Battery Performance Evaluation

The performance of ZABs is generally measured using two parameters: activity and rechargeability. The activity of ZABs is assessed by discharge–charge voltage polarization and power density, which are influenced by the bifunctionality of the electrocatalyst [37, 58]. Rechargeability (or cycle ability) reflects the stability

and durability of bifunctional electrocatalysts and is determined by the lifetime of ZABs in cycling tests at various current densities [59, 60]. The growth of the anode dendrite and electrolyte loss or leakage greatly constrains the cycling lifetime. The cathode is the most expensive part of the battery, and it strongly influences the performance and longevity of the battery. In the following section, we have discussed bifunctional electrocatalysts at the cathode (Figs. 1, 2 and 3).
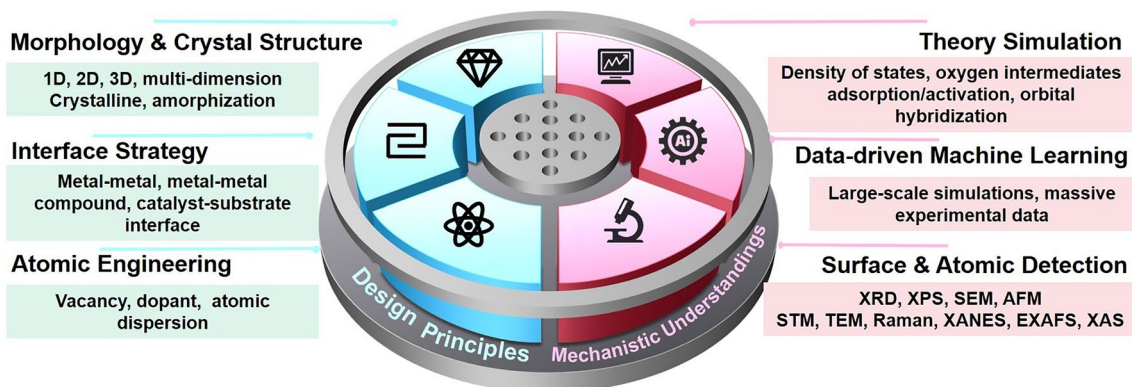

Fig. 1 The scope of this review, which covers three aspects in the sequence of catalysts and analytical engineering
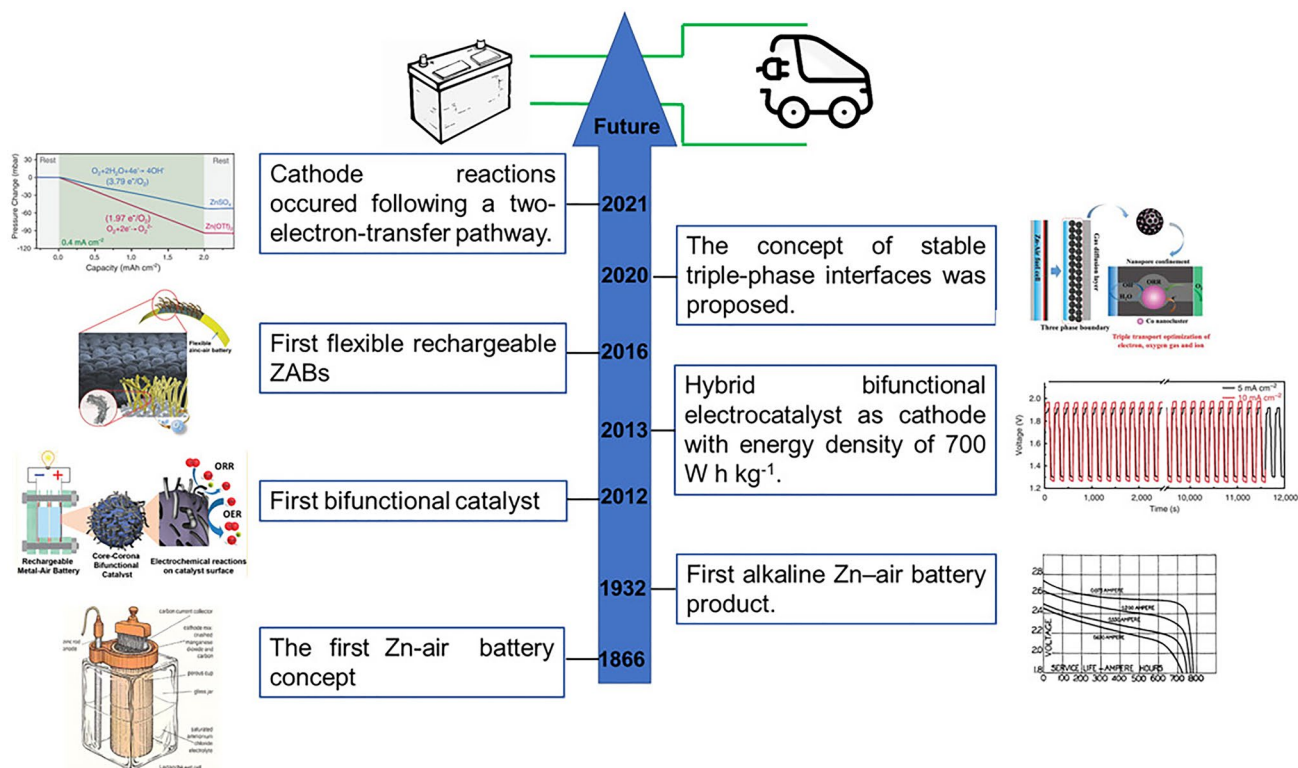

Fig. 2 Schematic illustration of the progress of zinc–air batteries. Reprinted with permission from Ref. [43, 44, 46–50]
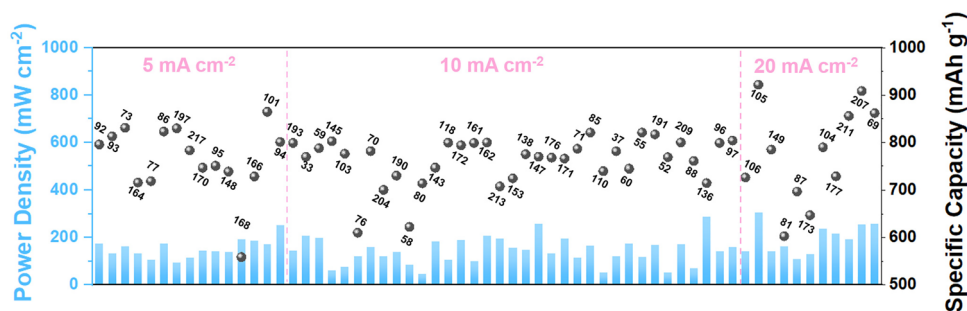
Fig. 3 The distribution of the performance of the reported bifunctional electrocatalysts in recent three years

4 Design Principles for Bifunctional Electrocatalysts in ZABs

The benchmark electrocatalysts are mostly made of precious metal materials, i.e., Pt/C for ORR and RuO_2/IrO_2 for OER. However, these noble-metal materials are expensive, scarce, and do not exhibit high catalytic performance for ORR and OER. Therefore, research on efficient and cheap bifunctional electrocatalysts is necessary (although challenging) for commercializing ZABs. In this section, the contemporary bifunctional electrocatalysts are divided into three major categories, including carbon materials, metal compounds, and metal/carbon hybrids. To provide an overview of this field and drive future research, a thorough and methodical recapitulation of bifunctional capabilities is necessary. Data on catalysts has been collected and statistically analyzed in recent years to determine the distribution of electrocatalytic performance and guide the rational design of future electrocatalysts. All summarized data are presented in Fig. 3, which shows the electrochemical performance restricted within a power density and specific capacity of 300 mW cm^{-2} and 950 mAh g^{-1}, respectively. Although significant progress has been made, the performance of ZABs, especially the activity of the ORR and OER at the cathode, is still challenging.

Oxygen electrocatalysis occurs at the triple-phase region, where the electrocatalyst contacts the electrolyte and O_2. To develop an efficient bifunctional electrocatalyst, two general design principles are mainly considered at the triple-phase boundary. The first one involves increasing the number of active sites on the surface, which is usually achieved by increasing the catalytic surface area or optimizing the porosity of electrocatalysts. The other one involves altering the configuration of the active sites and manipulating the

electrocatalytic efficiency of single sites. The ideal non-noble-metal bifunctional electrocatalysts for ZABs should be highly porous, inexpensive, eco-friendly, and have an optimal bond strength between zinc cations and oxygen/hydroxide species, small steric hindrance during charge transfer, superior conductivity, excellent chemical, and structural stability in the electrolyte, and a high surface area.

To summarize, recent advancements made in the design principles for ZAB cathode electrocatalysts fall under four main categories: (1) morphology design, which encompasses aspects such as shape, size, facet, porous size, and surface roughness; (2) crystal structure tuning, which pertains to crystalline and amorphous types; (3) interface strategy, which is beneficial to create or improve the catalytic activity, even accelerate the mass diffusion/charge during the electro-catalytic process; (4) atomic engineering, which involves techniques such as creating vacancies and dopants, as well as, atomic dispersion. These four methods can also interact and compound with each other. For example, shape and defects can both increase the surface area, which can increase the number of active sites. Facets and dopants can improve conductivity and enhance the stability of ZABs.

4.1 Morphology Design

Geometrical merits attribute the superior performance of ZABs to the high specific surface area, beneficial architecture, and secondary structure. Specifically, the high surface area provides abundant electrocatalytic sites, and the pore structure favors electrolyte penetration. The secondary or hierarchical morphology can contribute to preserving the structural integrity and, therefore, to maintaining high electrocatalytic stability [61–65]. The different nanostructures can facilitate advancements in various ways.

Based on previous geometrical assessments, a wide range of structures was obtained, including zero-dimensional nanoparticles, one-dimensional (1D) nanorods/nanofibers/ nanotubes, two-dimensional (2D) nanosheets/nanoplates, and three-dimensional (3D) hierarchical structures. A multidimensional composition is also a common approach to morphology design.

4.1.1 Zero-dimension

Quantum dots (QDs), with sizes below 10 nm, have recently emerged as a pioneering class of nanomaterials, exemplifying the characteristics of 0D materials [66]. Among these, carbon quantum dots, ranging in diameter from 5 to 20 nm, have been extensively investigated for their role as metal-free electrocatalysts in ORR [67]. In a noteworthy contribution, Fan et al. demonstrated the synthesis of graphene quantum dots at low temperatures, employing a facile method that yielded a uniform nanometer-sized distribution, as visually depicted in Fig. 4a, b [68]. It's crucial to emphasize that quantum dots seldom exist independently; rather, they are typically integrated onto a carrier platform. A more comprehensive exploration of this phenomenon will be presented in the upcoming Multidimensional Composition Sect. 4.1.5. This section aims to delve deeper into the synergistic effects and multifaceted compositions that arise when quantum dots are coupled with specific carriers, providing a holistic understanding of their functional roles in various applications.

4.1.2 One-dimension

One-dimensional materials, encompassing nanofibers, nanowires, and nanotubes, serve as versatile building blocks with a multitude of applications [69], particularly in various energy storage-related contexts [70, 71]. Their distinctive electrical and optical properties, coupled with a high specific surface area, confer substantial advantages over traditional materials [72, 73]. In an insightful study, Li et al. successfully synthesized a one-dimensional hierarchical ternary nanocomposite of MnO@CNT@Co through a facile single-step calcination reaction. The porous 1D hierarchical nanostructure, in tandem with multiple active sites, collectively contributes to the exceptionally high bifunctional electrocatalytic performance and efficiency of MnO@CNT@Co in catalyzing both ORR and OER [74]. In a parallel effort, Li et al. employed a molten salt template method to synthesize one-dimensional $La_{0.8}Sr_{0.2}Mn_{0.95}Co_{0.05}O_3$ nanowires, as illustrated in Fig. 4c, d. The introduction of doped-Co in the nanowires resulted in the alteration of the band center of O $2p$, Mn $3d$, and Co $3d$, effectively reducing the energy barriers of oxygenated intermediate species [75]. This strategic modification underscores the significance of tailoring the composition of one-dimensional materials to achieve optimized electrocatalytic performance in energy-related applications.
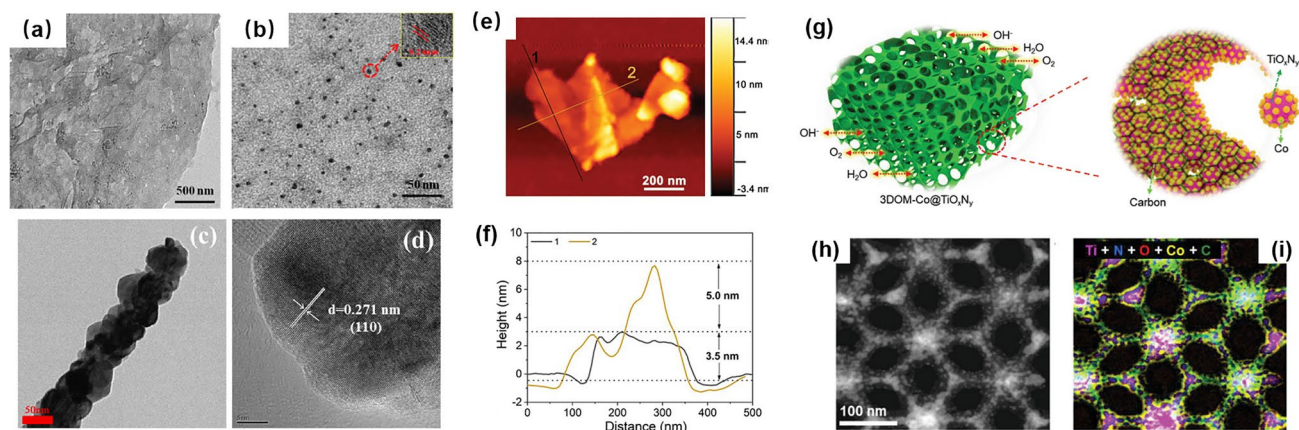

Fig. 4 a TEM and **b** HRTEM images of the graphene quantum dots. Reprinted with permission from Ref. [68]. **c** TEM and **d** HRTEM of 1D $La_{0.8}Sr_{0.2}Mn_{0.95}Co_{0.05}O_3$ nanowires. Reprinted with permission from Ref. [75]. **e** AFM image and **f** the corresponding height profiles of CoO nanosheets. Reprinted with permission from Ref. [63]. **g** Schematic illustration and **h** STEM image, and **i** elemental mapping (Ti, Co, O, N, and C) of 3DOM titanium oxynitride. Reprinted with permission from Ref. [87]

4.1.3 Two-dimension

Two-dimensional (2D) atomically thin catalysts are ideal platforms for ORR and OER [76, 77]. They have certain advantages, for example, (1) the charge distribution in the unique layer structure facilitates electron transfer; (2) the thin structure and strong in-plane chemical bonds improve the catalytic activity and offer superior mechanical strength; (3) the strong in-plane bonds with the thin structure offer superior mechanical strength; (4) the large aspect ratios (thin-layer) and the large number of exposed atoms on the surface provide a large specific surface area and a large number of active sites; (5) the 2D architecture provides a feasible and ideal model to modify its electronic distribution [78–82]. The CoO nanosheets fabricated by Tian et al. (Fig. 4e, f) were thin and had a high specific surface area and sufficient atomic utilization, leading to high rates of ORR/OER [63]. Many researchers use 2D MXenes as cathode materials in ZABs because they have high electrical conductivity, hydrophilicity, and mechanical strength. These properties facilitate efficient electronic charge transport at the electrode–electrolyte interface and promote fast Zn^{2+} diffusion, which greatly improves electrode kinetics, as proposed by Huang et al. [83].

4.1.4 Three-dimension

The development of three-dimensional (3D) physical structures has facilitated the emergence of new phenomena, such as restructuring and multiscale effects, which are attributed to the microstructure, dimensionality, and morphology of the materials [84–86]. Liu et al. synthesized 3D ordered microporous (3DOM) titanium oxynitride (Fig. 4g–h), in which the large diffusion channels for oxygen species and highly accessible active sites facilitated mass transfer; they were also quite durable [87]. Inspired by the former research, similar work by Wang et al. reported 3D ordered microporous P-doped Co_3O_4 (3DOM P-$Co_3O_{4-\delta}$) [88]. Deng et al. found that the core–shell structure enhances the accessibility of active sites and widens the channels, which facilitates the diffusion of oxygen species. By encapsulating (Mg, Co)$_3$O$_4$ in N-doped graphitized carbon, the researchers recorded a highly efficient bifunctional oxygen electrocatalytic activity that outperformed even the most advanced noble-metal benchmarks [89]. Metal–organic frameworks (MOFs) with porous structure, high surface area and increased number of active sites, have attracted great interest of researchers [90]. Wang et al. designed porous cake-like ZnMn–NC by loading Mn into Zn–MOF and pyrolysis, resulting in an enhanced ORR activity [91]. The 3D electrocatalysts with many exposed active sites accelerated the activation of reactants/intermediates, and the irregular morphological features optimized the triple-phase interface [92, 93].

4.1.5 Multi-dimension

In multidimensional composite catalysts, different types of materials or structures are combined to create a composite structure with enhanced catalytic properties [94, 95]. Multidimensional composite catalysts are used extensively as they have higher catalytic activity, better selectivity, and improved stability than traditional catalysts [96, 97]. For example, Guo et al. introduced graphene quantum dots into Ni–Fe-layered double hydroxides as an air cathode for ZABs. The electrostatic adsorbing effect of graphene quantum dots improved the OER [98]. Another example was reported by Xu et al., who developed a facile hydrothermal and pyrolysis procedure to prepare Ni_3S_2 quantum dots on carbon nanosheets (Fig. 5a, b). By using this methodology, the robust bifunctionality of the air cathode exhibited ultra-long cyclability with a high discharge capacity, which probably resulted from the quantum size effects, oxygen deficiency, and a porous texture [99]. Wang et al. synthesized black phosphorus nanosheets with graphitic carbon nitride (denoted BP-CN-c) (Fig. 5c) with a mean thickness of 3.7 ± 1.3 nm using an electrochemical delamination method, which exposed the atoms and active lone pair electrons to promote the adsorption of OOH* [100]. One-dimensional structures provide more surface area and better transmission channels, while three-dimensional structures offer more reaction sites and greater stability. By combining these two structures, the catalytic efficiency and selectivity of a catalyst can be further improved, while reducing the toxicity and cost of the catalyst [101]. This can help in meeting the needs of different catalytic reactions. Some researchers synthesized a 3D nano-forest architecture composed of CoFe alloy and 1D N-doped CNTs grown on carbon nanofibers via electrospinning and two-stage
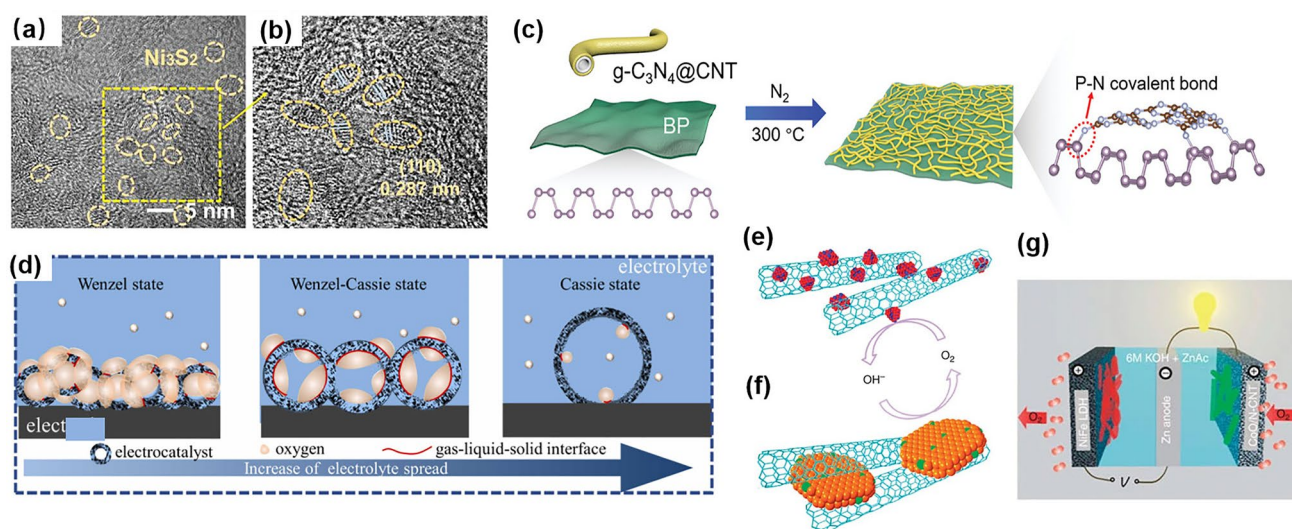
Fig. 5 **a**, **b** HRTEM images of Ni_3S_2 quantum dots. Reprinted with permission from Ref. [100]. **c** Schematic illustration of 2D BP-CN-c. Reprinted with permission from Ref. [99]. **d** A diagrammatic representation of electrolyte diffusion state on hollow CoFe–NC–x. Reprinted with permission from Ref. [102]. **e**–**g** CoO and Ni–Fe-layered double hydroxide with CNT hybrids for the electrocatalysis of ORR and OER. Reprinted with permission from Ref. [47]

heat-treatment [102]. The as-prepared CoFe@NC had a stable 3D structure, high conductivity, and hierarchical pores, which imparted high power density, low voltage polarization, and stable cycling compared to commercial ZABs (Fig. 5d). Zhuang et al. also reported similar findings; they described how the substantial surface curvature within mesoporous hollow spheres can produce a fortified air pocket and strengthen the air cushion when submerged underwater. Conversely, the reduced curvature resulting from an increased internal diameter can promote gradual electrolyte infiltration. Further experiments showed that the rapid entry and exit of reactants and products on an optimized triple-phase interface facilitated a low Tafel slope of ORR [103]. Dai et al. developed a hybrid oxygen reduction catalyst consisting of CoO and carbon nanotubes and an oxygen evolution catalyst made from Ni–Fe-layered double hydroxide and used them as cathodes (Fig. 5e, f). They conducted preliminary experiments on rechargeable Zn–air batteries using a tri-electrode setup. In this setup (Fig. 5g), OER and ORR electrocatalysts were applied to two separate electrodes for charging and discharging, respectively. The ORR electrode was connected only to the Zn anode for discharging, which prevented exposure to positive potentials. This configuration allowed for the decoupling of the two electrocatalysts, which enabled individual optimization [47].

By combining the advantages of different dimensional structures and materials, multidimensional composite catalysts can significantly enhance the catalytic activity and stability of ORR and OER [94, 104]. Additionally, the design and synthesis of multidimensional composite catalysts can be tailored for specific applications by controlling the composition, structure, and morphology of the catalysts [105, 106]. However, further studies are needed to elucidate the underlying mechanisms and optimize the performance of multidimensional composite catalysts for practical applications.

4.2 Crystal Structure Tuning

4.2.1 Crystalline

The crystal structure of electrocatalysts strongly influences electrocatalytic processes, and the rational tuning of the surface structure to expose the active sites can enhance the performance of ZABs [107–110]. For example, Li et al. described a general method for synthesizing ultrafine Co-Mn spinel with cubic (c-spinel) and tetragonal (t-spinel) crystallographic symmetry. Compared to t-spinel, c-spinel contains more catalytic sites and a higher average oxidation state of Mn (> 3), which results in stronger binding of O_2 molecules and improves electron conduction (via

hopping) and charge transfer (through redox reactions), thus favoring electrocatalysis [111]. Lee et al. examined spinel-structured oxides (Co_3O_4, $(Ni, Co)_3O_4$, and $(Mn, Co)_3O_4$), which exhibited different levels of catalytic activity for both ORR and OER. The degree of activity depended on the transition metal (Co, Ni, and Mn) that was inserted into the octahedral sites of the spinel lattice [112]. Zhao et al. synthesized FeCoNC with two distinct structures, including star-like and dodecahedron-like structures. The star-like catalysts had a greater specific surface area than the dodecahedron-like catalysts due to their intricate structure. The unique structure allowed the star-like catalysts to expose more active sites, thus enhancing their catalytic activity for both ORR and OER (Fig. 6a, b) [113].

Due to the unique coordination environment and properties of different facets, specific facets with low activation barriers might be exposed to achieve maximum activity toward oxygen reactions [114, 115]. The (112) high-index facet has a more open structure with higher stepped atom density and density of catalytic active Co^{3+} sites compared to the (001) and (111) facets. Han et al. synthesized Co_3O_4 nanocrystals enclosed by the (001), (001) + (111), and (112) planes and found that the Co^{3+}_{Oh} species on the (112) plane acted as superior active sites

in terms of adsorption, activation, and desorption, as determined by DFT calculations (Fig. 6c–e) [116]. In another study, Xie et al. fabricated Ni–Fe alloy nanoparticles with (111) and (200) facets and found that the Zn-air batteries exhibited superior performance when assembled with (200)-faceted nanoparticles, due to the significantly high compressive strain exerted by these particles (Fig. 6f, g) [117].

While exposing specific facets can enhance the activity of electrocatalysts for ZABs, it can be challenging to maintain the crystal state of the catalysts throughout the electrochemical test. This is because the preferential orientation of the facet in catalysts often leads to the presence of grain boundaries, defects, and other factors that can also strongly influence the performance of ZABs [118]. Additionally, catalysts are sensitive to the reaction condition and might undergo irreversible reconstruction during preparation and reaction. In situ characterization can help distinguish the evolution of crystal structure and facets; In situ techniques are discussed later as a new concept.

4.2.2 Amorphization

Amorphization in an electrocatalyst increases the number of unsaturated coordination sites, which can improve the
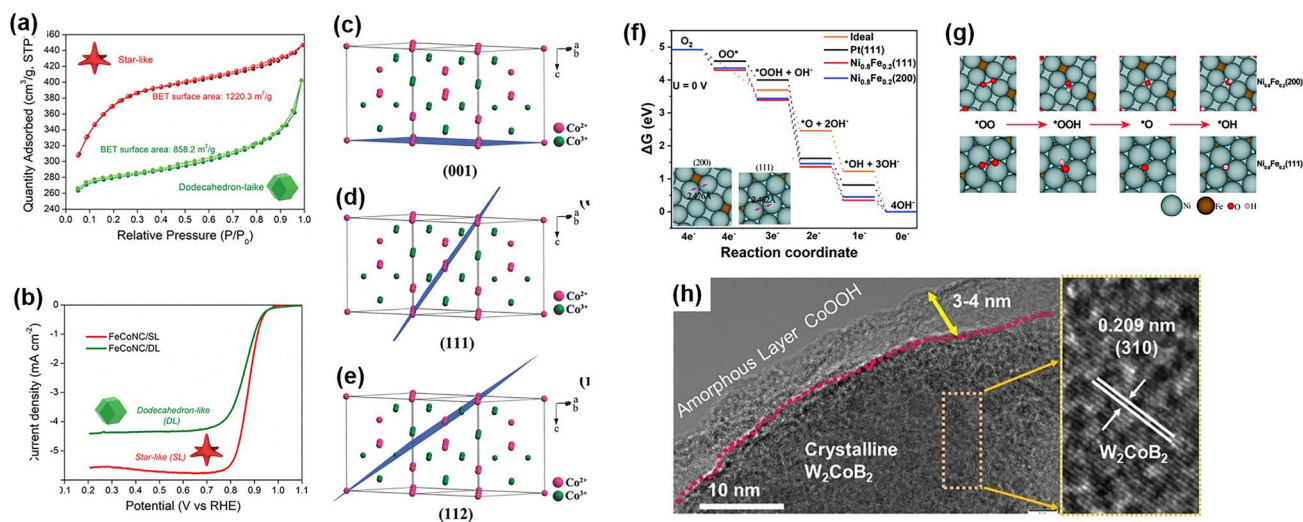

Fig. 6 **a** The BET surface areas and **b** LSV curves of ORR of FeCoNC with star-like and dodecahedron-like structures. Reprinted with permission from Ref. [113]. **c–e** The Co^{2+}/Co^{3+} surface atomic configurations and the corresponding side views of calculated O_2-adsorption matter on different planes. Reprinted with permission from Ref. [116]. **f, g** Gibbs free energy and processes related to the ORR steps on the (111) and (200) facets of $Ni_{0.8}Fe_{0.2}$. Reprinted with permission from Ref. [117]. **h** TEM and HRTEM images of crystalline W_2CoB_2 with amorphous CoOOH layer. Reprinted with permission from Ref. [133]

catalytic activity more effectively than the crystalline form [119, 120]. However, amorphous materials generally have poor conductivity and need to be loaded, deposited, or grown on conductive supports like carbon materials to facilitate electron transport and enhance electrical conductivity, which can result in lower ORR/OER overpotentials [121, 122].

Xu et al. reported the synthesis of Cu nanocluster/FeN$_4$ amorphous composites embedded in N-doped graphene (Cu/Fe–NG), which has an amorphous structure that provides abundant and accessible active sites critical for the boosted ORR activity [82]. Amorphous oxides based on Fe, Co, or Ni with unparalleled 3d orbits showed excellent ORR performance, compared to the ORR performance of their corresponding crystalline counterparts. Carbon materials also have abundant active sites for the nucleation of oxides and avoid agglomeration. Liu et al. prepared a NiFePO–C composite as a cathode catalyst for ZABs, which showed stable cycling for more than 100 h [123]. Amorphous catalysts generally possess a large number of vacancies formed by lattice defects and disordered structures, which provide isotropic ion diffusion pathways and superior electrocatalytic performance [124]. Specifically, layered CoO (L–CoO) with long-range disorder structures have abundant ample oxygen vacancies and abundant oxygen chemisorption sites; these greatly enhance the ORR and OER performance and improve electrical conductivity [125].

Several studies used metal carbides (WC [126], TiC [127], Mo$_2$C [128], B$_4$C [129] etc.) and metal borates (M–B) as substrates as they exhibited excellent ORR/OER performance, owing to the large negative charge and electronic adjustment in the electrochemical processes [130, 131]. For example, Zhao et al. synthesized an amorphous electrode with iron borate nanolattice on the surface of nickel foam, in which the borate anions modified the electronic structure of transition metals and accelerated oxygen reactions [132]. Based on their findings, Saad et al. embedded crystalline W$_2$CoB$_2$ into the amorphous CoOOH layer (Fig. 6h), which resulted in high OER performance [133].

In spite of the commonly reported progress in ORR/OER catalytic activity, the working principle of amorphous composites in boosting the ORR/OER is still unclear. The current working theory is based on a combination of the following: (1) the electronic structure of metal sites is tailored by amorphous composites, and the electrocatalytic

reaction barrier can be modified; (2) the vacancies can act as reaction sites and enhance the reaction kinetics [134, 135]. In addition, amorphous materials suffer from poor chemical and structure stability, which hinders the practical applications in ZABs.

4.3 Interface Strategy

Rechargeable ZABs rely on a gas–liquid-solid triple-phase electrochemical reaction, where the surface/interface of the electrocatalyst is essential for determining the density, electrical conductivity, and reaction energy barrier of the exposed active site [136, 137]. Thus, the surface/interface of the electrocatalyst influences the performance of rechargeable Zn-air batteries.

The interface can be divided into the metal–metal interface, the metal–metal compound interface with the same or different metal, and the catalyst-substrate interface. The Co/CoFe heterointerface developed by Niu et al. is an excellent illustration of how metal–metal interfaces can enrich catalytic active sites and promote charge transfer between different components, which in turn can enhance electrocatalytic performance [138].

The metal–metal compound interface at the atomic scale can greatly enhance catalytic performance due to a synergistic effect. Many researchers have investigated interfacial interactions for the ORR/OER. Jiang et al. synthesized a hybrid material composed of interpenetrating metallic Co and spinel Co$_3$O$_4$ "Janus" nanoparticles. The interfaces between the two components served as atomic traps that imparted exceptional adsorption capability for adsorbing oxygen reactants (Fig. 7a, b) [139]. Baeck et al. prepared well-defined heterointer-faces between CoFe alloy and spinel-type CoFe$_2$O$_4$. The DFT calculations showed that the development of strongly coupled heterointerfaces between the CoFe alloy and n-type bimetal oxide (CoFe$_2$O$_4$) can generate a Mott-Schottky barrier, which can induce band structure bending and facilitate spontaneous electron transfer from the CoFe alloy (which has a higher work function) to CoFe$_2$O$_4$ (which has a lower work function) (Fig. 7c, d), thus enhancing the catalytic activity [140]. Wu et al. found that a heterogeneous interface of multicomponent cobalt oxides can generate rich oxygen vacancies as active sites, which can combine with the mixed valence of Co^{2+} and Co^{3+} to
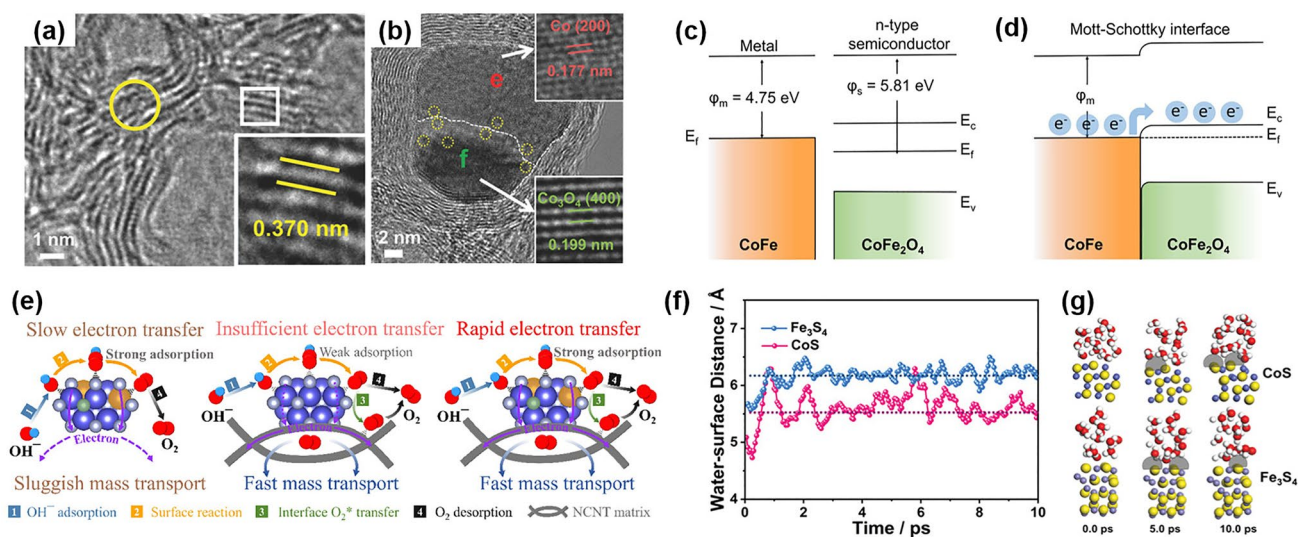
Fig. 7 **a**, **b** HRTEM images of the interface between Co and Co_3O_4. Reprinted with permission from Ref. [139]. Energy band of CoFe alloy and $CoFe_2O_4$ **c** before and **d** after Mott-Schottky contact. Reprinted with permission from Ref. [140]. **e** Schematic illustration of electron and mass transport during the OER process on FC–Ni_3N (left), Ni_3N/NCNT (middle) and FC–Ni_3N/NCNT (right). Reprinted with permission from Ref. [144]. **f** AIMD simulations of water layers on CoS and Fe_3S_4. Reprinted with permission from Ref. [146]

produce a Co/CoO/Co_3O_4/NCS catalyst with high ORR/OER performance [141]. Transition metal phosphides were found to be a promising class of oxygen electrocatalysts. Niu et al. developed a hetero-structural hybrid with a closely integrated CoO/Co_xP interface that increased the accessibility of active species and facilitated smooth electron/reactant transportation. Because of these features, the newly-developed electrocatalyst outperformed the state-of-the-art non-noble-metal catalysts and even noble-metal benchmarks [142]. Guo et al. developed a Cu_3P/TiO_2 interface to optimize the adsorption of oxygen intermediates, shorten the electronic/mass transport path, and enhance the kinetics of the ORR reaction [143].

In electrocatalysis, the interface between the catalyst and the substrate is also significant. For example, Lu et al. anchored Ni_3N onto the surface of NCNT to create a heterointerface, which increased the transport of electrons and oxygen between Ni_3N and the conductive NCNT matrix (Fig. 7e) [144]. Similarly, Li et al. embedded Co nanoparticles in N-doped carbonized wood (Co@NCW). The interface between Co nanoparticles and N-doped graphitic carbon shells provided a fast electron transfer pathway at the interface and produced a synergistic effect that enhanced the electrocatalytic performance [145]. Yan et al. developed a hydrophobic-aerophilic strategy to fabricate CoS/Fe_3S_4 nanoparticles encapsulated in

S, N co-doped carbon plate arrays. They found that the hydrophobic-aerophilic surface of the S, N co-doped carbon plate arrays created a favorable environment for the CoS/Fe_3S_4 nanoparticles to exhibit excellent OER activity. The ab initio molecular dynamics (AIMD) simulations showed that the hydrophobic surface repelled water molecules, creating abundant solid–liquid–gas three-phase reaction interfaces, while the aerophilic surface exposed Fe-sites and promoted the diffusion of reactive molecules/ions across the interface and the adsorption of oxygen (Fig. 7f) [146].

Interfacial catalysis is extensively applied in ZABs and shows satisfactory performance [147]. Although many studies have investigated the role of interfaces in electrocatalysis, there is still no consensus among researchers on the actual active center. Hence, whether the active center is the interface, the compounds formed at the interface, or the disorder/vacancies created by the interface is unclear. Further studies should be performed to better understand the underlying mechanisms of electrocatalysis at the interface. Researchers also need to assess the controllable interface and quantify the density of the interface to optimize the performance of ORR and OER.

4.4 Atomic Engineering

4.4.1 Vacancy

Vacancy engineering is performed to enhance catalytic activity by removing atoms from the bulk catalysts, which can modify the electronic structure of adjacent atoms [148, 149]. The oxygen vacancy (V_O) is the most common type of deficiency, which can serve as an active site in oxygen electrocatalysis and enhance electrical conductivity and the adsorption of reactants [150]. To understand the relationship between V_O and ORR/OER performance, Tian et al. prepared various $NiCo_2O_4$-based mesoporous nanosheets (PNSs) with different levels of V_O by adjusting the calcining time. The concentration of V_O can be determined by performing X-ray photoelectron spectroscopy (XPS) and extended X-ray absorption fine structure spectroscopy (EXAFS) (Fig. 8a, b) [151]. The DFT calculations indicated that the activation energy of the rate-limiting step of ORR and OER was lowered by abundant V_O. The results of the electrochemical tests showed that appropriate oxygen vacancies can promote electrochemical activity, but excessive oxygen vacancies can cause morphological changes and structural collapse,

resulting in a decline in performance [151]. Heteroatom doping can enhance oxygen vacancies, as reported by Qin et al. Co single atoms on N-doped graphene can induce oxygen vacancy, which can regulate the charge density and optimize the electronic structure of Co sites. This can help in producing an optimal electrocatalyst with reduced overpotentials for both ORR and OER (Fig. 8c, d) [152].

Introducing other atom vacancies can also modulate the electrocatalytic performance of nanomaterials [153]. For example, Lai et al. reported an in situ CN vacancy developed by N_2-plasma activation of NiFe-PBA catalysts. Raman and electron spin resonance (ESR) spectra were used to confirm the presence of V_{CN} (Fig. 8e, f) [154]. Song et al. synthesized nickel hydroxide with adjustable levels of nickel vacancies (V_{Ni}) and showed that V_{Ni} significantly helped in the transformation of $Ni(OH)_2$ into active NiOOH species [155].

Vacancy defects are also used to generate intrinsic vacancies and alter grain boundaries, which can provide feasibility to regulate their structure and enhance activity [156]. This is usually achieved via high-temperature treatment, chemical etching, or decreasing thickness. For example, Tao et al. produced edge-rich graphene by Ar-plasma etching and found
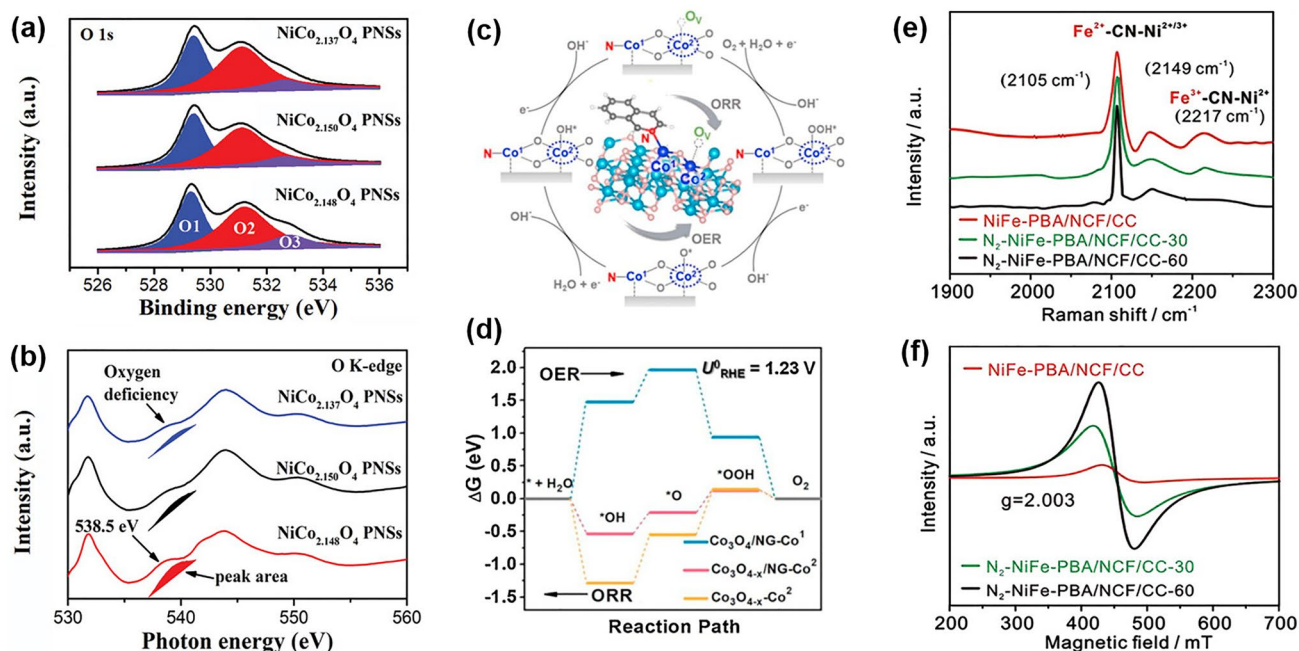

Fig. 8 **a** O 1*s* spectra and **b** O K-edge XANES spectra for $NiCo_{2.148}O_4$, $NiCo_{2.150}O_4$, and $NiCo_{2.137}O_4$ PNSs. Reprinted with permission from Ref. [151]. **c** ORR and OER mechanisms over Co_3O_4-x/NG. **d** The calculated free energy diagram of ORR/OER for three different Co sites. Reprinted with permission from Ref. [152]. **e** Raman and **f** ESR spectra of different NiFe samples. Reprinted with permission from Ref. [154]
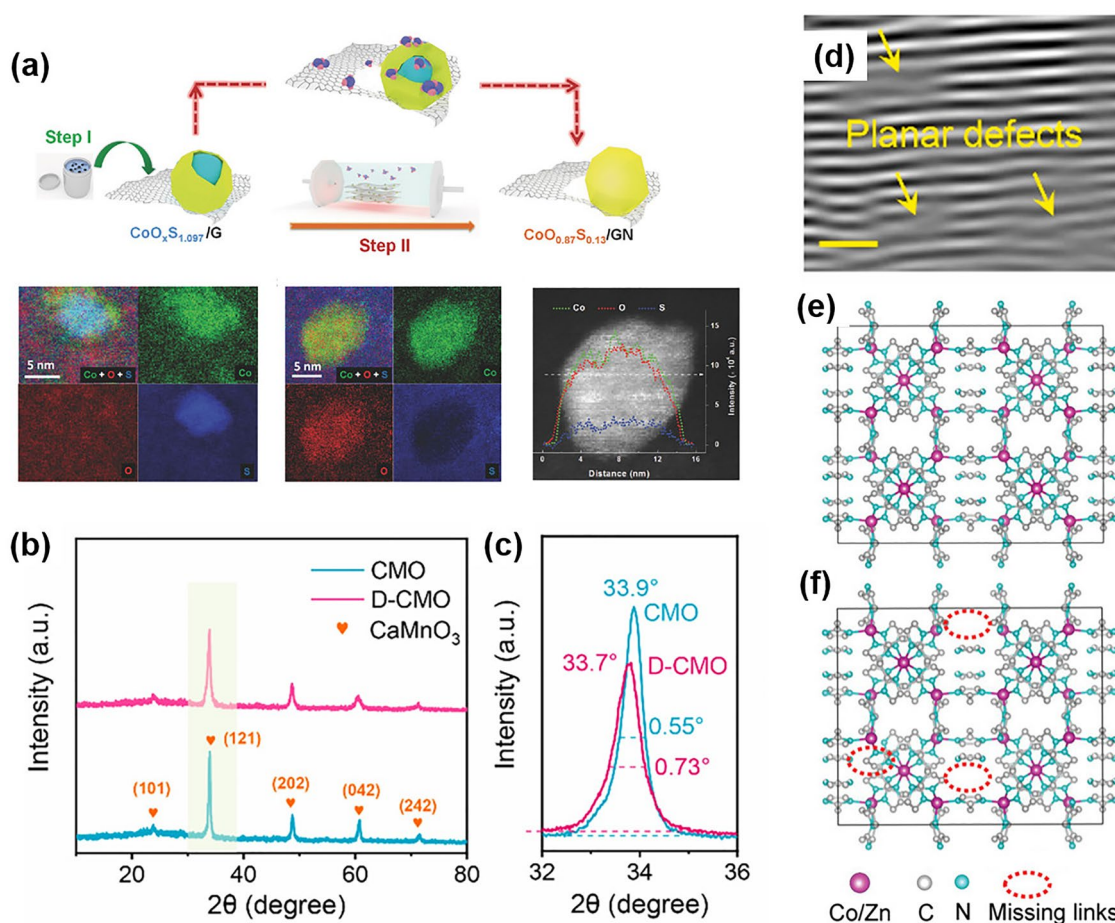
Fig. 9 **a** Schematic illustration of the synthesis of $CoO_{0.87}S_{0.13}$/GN. Reprinted with permission from Ref. [158]. **b**, **c** XRD patterns, **d** FFT image of D-CMO. Reprinted with permission from Ref. [159]. Schematic diagram of the **e** intact ZIFs and **f** linker-deficient ZIFs. Reprinted with permission from Ref. [160]

that the edge-rich graphene had higher oxygen adsorption energy and more catalytically active sites for ORR than pristine graphene, determined by DFT calculations [157]. Fu et al. used the ammonolysis method and created $CoO_{0.87}S_{0.13}$ on graphene with an abundance of surface defects (Fig. 9a). The combination of oxygen-vacancy-rich, nonstoichiometric cobalt oxysulfides, and edge-nitrogen-rich graphene nanomeshes results in high electrocatalytic performance for ORR and OER [158]. Regarding high-temperature treatment, some phase transformations usually occur along with disordering of the crystal properties to some extent by controlling the calcination parameters. Yang et al. described a method to improve the activity of $CaMnO_3$ (CMO) by ammonia heat treatment to perform the octahedral deformation of CMO (denoted as D-CMO, Fig. 9b–d) [159]. Some researchers performed theoretical calculations and found that the surface

electron redistributions induced by octahedral distortion can lead to strong σ-type electronic coupling between the surface and adsorbents, which can enhance the ORR/OER activity of D-CMO, as the highest occupied molecular orbital (HOMO) and the lowest unoccupied molecular orbital (LUMO) are mainly distributed on this surface. Similarly, Yang et al. created linker defects in MOFs by removing some of the imidazole molecules from zeolitic imidazolate frameworks (ZIFs), which enhanced the activity of metal sites and electron transfer capability, resulting in outstanding bifunctional ORR and OER performance (Fig. 9e, f) [160]. It is essential to emphasize the intricate role of defects in electrocatalysis. Defects, while potentially contributing to beneficial effects, can also diminish activity. Additionally, they might function as recombination centers or undesired trap states.

4.4.2 Dopant

Many researchers have investigated and tested suitable doping elements for carbon substrates, as the electrically neutral carbon atoms of pristine carbon have poor activity toward the oxygen reactions [161, 162]. After the heteroatoms (N [163, 164], P [165, 166], B [167, 168], S [169, 170] etc.) doping, electrons are redistributed on nearby carbon atoms and act as the active sites for oxygen electrocatalysis. N-doping with various types of graphitic N, pyridinic N, pyrrolic N, and oxidized N has been extensively studied [171]. The type and concentration of N-doping in the carbon substrate are critical factors influencing the activity [172, 173]. For example, Lu et al. regulated pyridinic N (Pyri-N), graphitic N (Grap-N) and Amino- N on graphdiyne (GDY) via calcination temperature. With the concentration of pyri-N increasing, the ORR and OER performance have obvious advantages over other N-doped GDY catalysts, indicating pyri-N is the most favorable bonding mode for the oxygen reactions (Fig. 10a–c), being consistent with the results calculated by DFT [174]. Sun et al. prepared N, F co-doped porous carbon (NFPC) as bifunctional electrocatalysts for ZABs (Fig. 10d), where the DFT calculations showed a reduction in the depth of the local minima in the energy step diagrams, suggesting enhancement of OER and ORR [175].

The introduction of heteroatoms can sometimes regulate the local coordination environment [176, 177]. Meng et al. fabricated F, N-co-doped FeN_x moieties, which stabilized single Fe atoms and occupied vacancies during the defluorination process. This favored the adsorption of oxygen species and improved the performance of the oxygen reaction [178]. Zhou et al. investigated the effect of phosphorus on the electrocatalytic activity of FeN_4-based catalysts. The FeN_4 sites are the active sites for ORR, and their catalytic activity depends on the balance between the adsorption of *OOH and *O species. The researchers found that the addition of phosphorus effectively balanced the adsorption of *OOH/*O, which enhanced the ORR activity of the catalysts (Fig. 10e, f) [179].

Moreover, topological defects are often induced by heteroatom doping [180, 181]. Although carbon materials have high conductivity, their non-polar surface interacts weakly with oxygen-containing feedstocks, which results in poor electrocatalytic activity. To address this issue, topological defects, such as edge sites, lattice reconstruction, and dangling groups, can be introduced to regulate the electronic structure of carbon materials and create adsorption sites for oxygen-containing intermediates [182–184]. Yu et al. synthesized nitrogen-doped graphitic carbon nanosheets with numerous lattice defects that could change the catalytic properties of carbon materials [185].
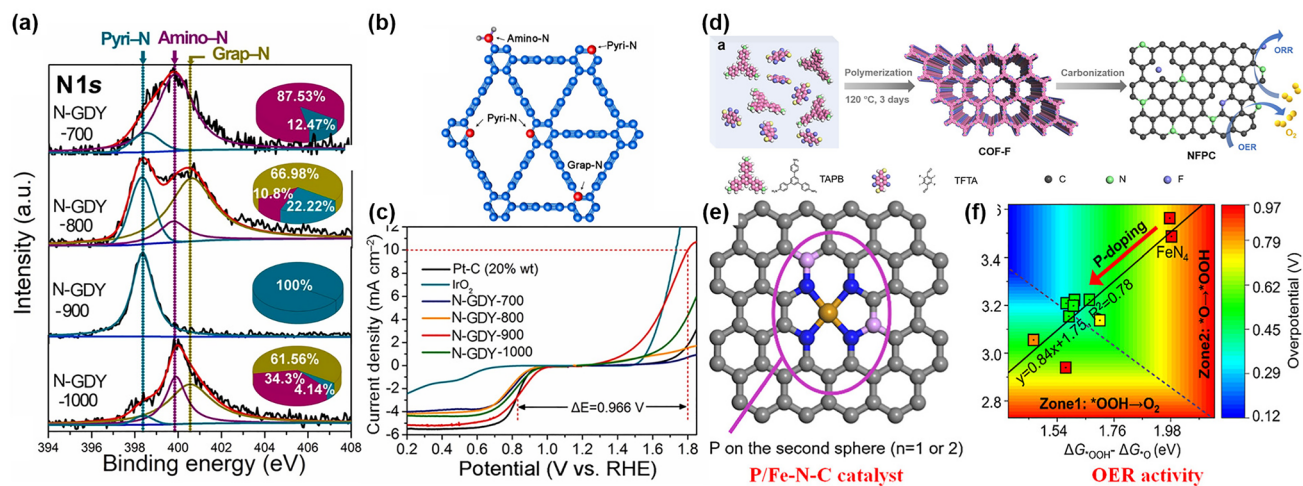

Fig. 10 **a** XPS spectra of N1s for the samples after calcination in different temperatures. **b** Diagram of different configuration of N doping. **c** ORR and OER performance of four catalysts compared with commercial Pt/C and IrO_2. Reprinted with permission from Ref. [174]. **d** Schematic illustration of the polymerization/crystallization of the COF-F and its subsequent carbonization for preparing NFPC. Reprinted with permission from Ref. [175]. **e** Schematic diagram of P/Fe–N–C catalyst. **f** Contour plot of OER overpotential as a function of Gibbs adsorption energies. Reprinted with permission from Ref. [179]

Besides the carbon materials, a series of transition metal compounds including oxides [186, 187], sulfides [188, 189], phosphides [190, 191] and nitrides [192] have exhibited their potential for the catalysis of ORR and OER. However, conventional transition metal compounds without modulation show poor electrocatalytic activity [193]. Doping strategies can effectively manipulate the electronic structure and tune intrinsic ORR/OER electrocatalytic activity [194–196].

For example, in a Co-doped NiO electrocatalyst, electron transfer between Ni and Co enhanced the electrocatalytic activity [197]. Besides simple metal oxides, doping principles are also effective in complex oxides, such as perovskites, spinel, etc. Chang et al. investigated the effect of substituting Fe, N, and P tri-dopant in carbon nanotubes on the enhancement of the catalytic activity of ORR. The DFT results indicated that a suitable amount of P dopants could modulate the local electronic structure near the active sites of the catalyst, thus improving the ORR performance. The P dopants altered the electronic properties of the catalyst, creating new active sites for oxygen adsorption and reducing the activation energy required for ORR. The P dopants also enhanced the stability of the catalyst by reducing the formation of harmful intermediate species in the reaction [198]. Sulfides have drawn extensive attention because they can effectively enhance OER activity through simple methods. Lyu et al. proposed a continuous heat-treatment strategy to synthesize N and S-modified Co_9S_8 as electrocatalysts. The modified Co_9S_8 catalysts showed considerably higher ORR and OER activity than the non-doped catalysts. This enhancement was attributed to the introduction of N and S, which led to an increase in the defect concentration, adjustment of the Fermi energy level, improvement of electronic conductivity, and optimization of the energy barrier for oxygen adsorption reactions [199].

4.4.3 Atomic Dispersion

Since 2011, the concept of atomic dispersion has gained popularity in the field of electrocatalysis [200]. It can maximize the efficiency of transition metal atoms by facilitating precise regulation and rational design of intrinsic ORR/OER activity [201, 202]. The dispersed atoms, typically arranged in an M–N–C structure, where M represents a transition metal such as Fe, Co, and Ni,

significantly improve the electrocatalytic activity even when present in small amounts [42, 203]. Some studies found excellent ORR catalytic performance of Co–N–C electrocatalysts [204–206]. Li et al. combined theoretical calculations and empirical findings to show that CoN_3 sites were more favorable for the four-electron transfer in the ORR process than CoN_4 sites [207]. Song et al. recently proposed a novel strategy to improve the performance of electrocatalysts by utilizing the synergistic effect between Co–N_2 and Co–N_4 moieties. The fully π-conjugated frameworks resulted from the presence of Co–N_2 and Co–N_4 moieties, which created a synergistic effect that enhanced the electronic conductivity and catalytic activity of the material [208]. Integrating multiple components in the composition of electrocatalysts allows for the selection of active sites for distinct mechanisms of ORR and OER, resulting in a generally superior bifunctional activity. Zhao et al. adopted this approach by selecting Co–N–C species and NiFe LDHs as ORR and OER active sites and integrating them into a composite (CoNC@LDH) for ZABs, which exhibited remarkable activity for both ORR and OER (Fig. 11a, b) [209].

Besides the Co–N–C active sites, M–N–C catalysts with different transition metal atoms at the center also exhibit acceptable catalytic activity [210]. Zong et al. synthesized M–N–C catalysts with different metal atoms at the center (M: Cu, Fe, Co, and Ni) on porous graphitic carbon nanospheres and found that Cu-SAs@N-CNS exhibited the highest ORR activity among the tested catalysts. The Cu–N–C catalysts showed exceptional electrocatalytic activity for both ORR and OER, making them highly efficient air cathode materials for ZABs [211]. Zhou et al. developed highly effective ORR catalysts in the form of atomically dispersed Mn-doped carbon materials (g-SA-Mn). The support for trapping and anchoring Mn-containing gaseous species was provided by porous zeolitic imidazolate frameworks. Through a high-temperature pyrolysis process, atomically dispersed Mn–N_x active sites were generated, which greatly enhanced the ORR catalytic performance of the material (Fig. 11c) [212].

The activity of pristine M–N–C sites can be enhanced by introducing a foreign metal site to create dual-atom catalysts [213]. Chen et al. placed nickel (Ni) and iron (Fe) single atoms on the inner and outer walls of graphene hollow nanospheres. The DFT calculations showed that
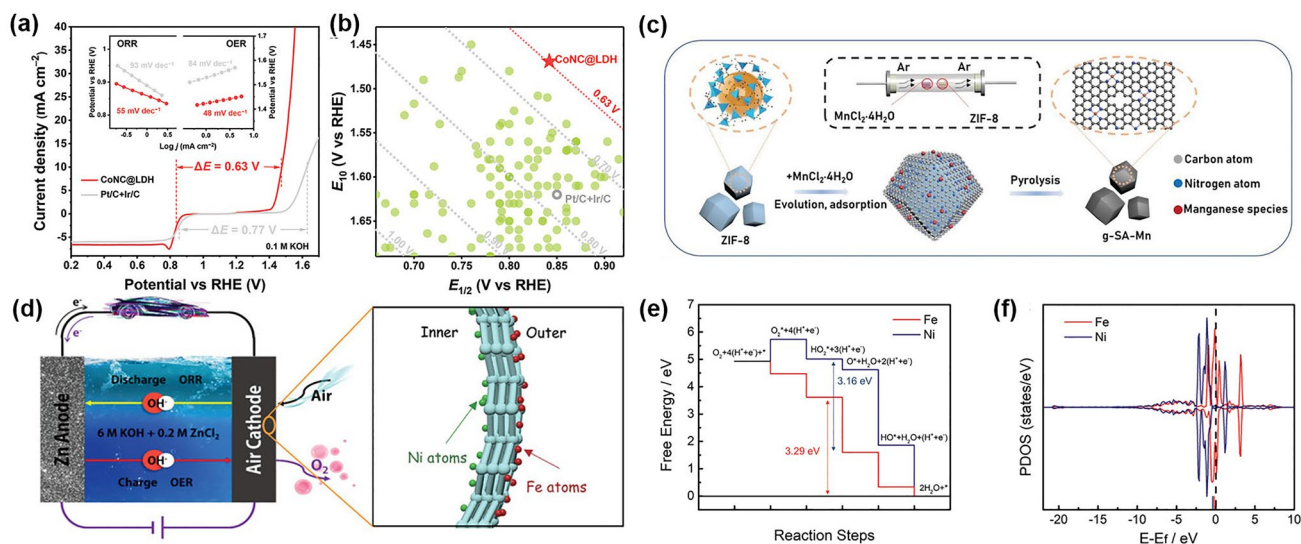
Fig. 11 **a** LSV curves and Tafel plots of the CoNC@LDH and Pt/C + Ir/C for ORR and OER, respectively. **b** Descriptor of ORR and OER activity among CoNC@LDH and other reported bifunctional electrocatalysts. Reprinted with permission from Ref. [209]. **c** Schematic illustration of the preparation of atomically dispersed Mn catalysts. Reprinted with permission from Ref. [212]. **d** A schematic diagram of a Zn–air battery assembled with Ni–N_4/GHSs/Fe–N_4. **e** Free energies of OER and f PDOS of the single-atom sites of Fe–N_4 and Ni–N_4. Reprinted with permission from Ref. [214]

the outer Fe–N_4 clusters significantly enhanced the ORR activity, while the inner Ni–N_4 clusters enhanced the OER activity (Fig. 11d–f) [214]. Wang et al. proposed a novel approach to optimize the electronic hybridization in Fe-based catalysts by introducing Se atoms. They also used DFT calculations to elucidate the underlying mechanisms of the observed phenomenon. The calculations suggested that the Se-doped Fe-based catalysts interacted strongly with the intermediates, which facilitated the adsorption and desorption of the intermediates during the catalytic process [215].

To summarize, the atomic dispersion structure has several advantages over other types of electrocatalysts, such as low metal dosage, high metal utilization, and uniform active sites. However, it has certain limitations, such as agglomeration and loss of single atoms during preparation and operation, which can lead to relatively poor stability.

5 Mechanistic Understanding of Bifunctional Electrocatalysts

Heterogeneous catalysis is the most common reaction in ORR and OER, in which the activity is accelerated by the used catalysts. It is important to develop a proficient catalyst and further for practical application. The improvement of

computing power and advanced techniques has facilitated intelligent and efficient exploration of the behavior of electrocatalysts. In this section, we described several typical computation descriptors and characterization techniques for catalysts. Through theoretical calculation and advanced characterization methods, the mechanism of bifunctional catalyst in ZABs was further analyzed.

5.1 Theory Simulation

The performance of electrocatalysts in enhancing ORR and OER can be analyzed through first-principle calculations based on DFT and spin-polarized computations, which can be performed using the Vienna ab initio simulation package (VASP).

The density of states (DOS) of the catalysts can be used to detect the conduction band, valence band, and band gaps, as well as defects; thus, it can be used for improving the electrocatalytic ORR/OER activity. The d-band theory can be used to determine how the catalyst can improve the activity [216]. For example, as shown in Fig. 12a, b, the upshift of ε_d from CoHZ to ZnHZ reflected the partial charge transfer from Zn to Co, which decreased the energy level of Co d-orbitals [24]. The study used DFT calculations to determine the electronic properties of the MOFs and elucidate the
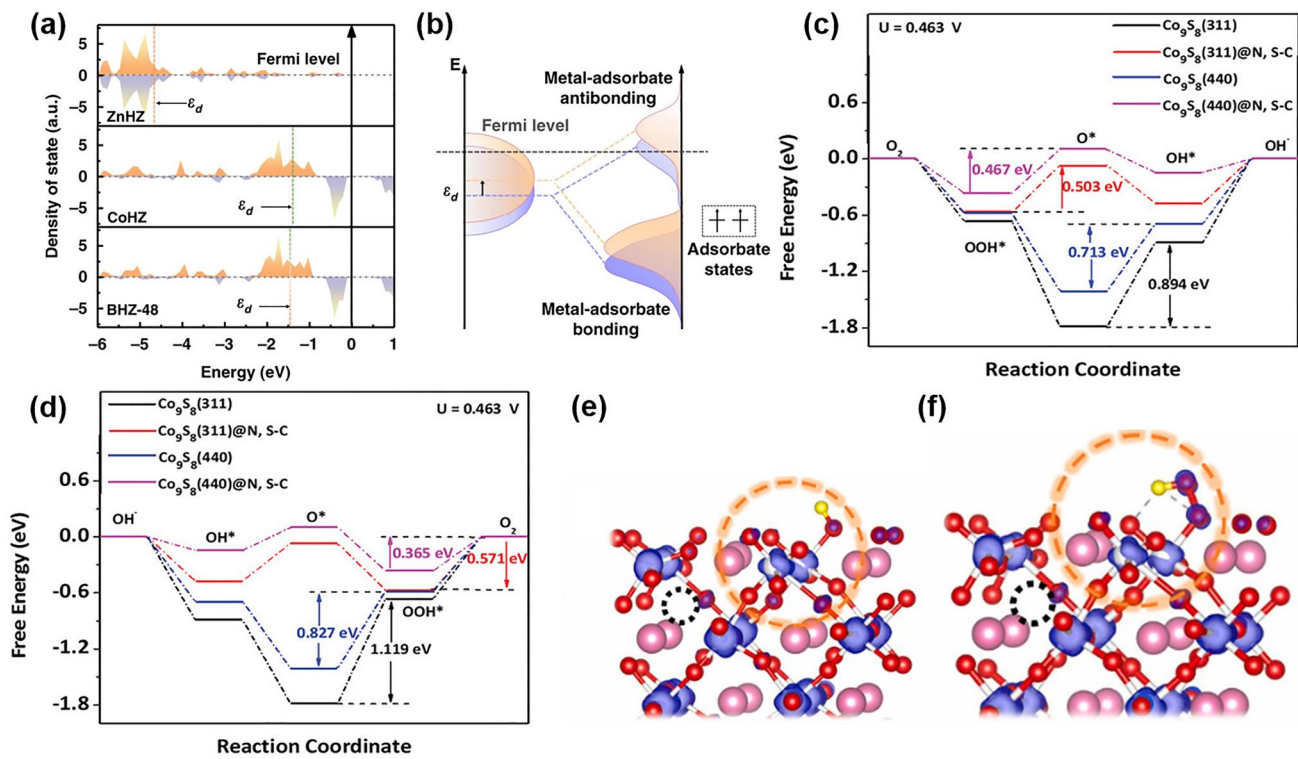
Fig. 12 a The calculated d band density of state for the transition metal atoms in ZnHZ, CoHZ, and BHZ-48. **b** Schematic illustration explaining change of metal adsorbate interaction by altering the metal d band center (ε_d). Reprinted with permission from Ref. [24]. Free energy diagram of various Co_9S_8 for **c** ORR and **d** OER pathways. Reprinted with permission from Ref. [199]. The HOMO of D-CMO (121) with **e** OH* absorption and **f** OOH* absorption, respectively. Reprinted with permission from Ref. [159]. FEM multiphysics modeling of O_2 diffusion and O_2 concentration contour near the **g** $CoS/Fe_3S_4@SNCP$ and **h** $CoS@SNCP$ air cathodes. **i** Three representative structures during AIMD simulations. Reprinted with permission from Ref. [146]

charge transfer mechanism. Additionally, the energy level of the p orbitals relative to the Fermi level is an important factor in determining the adsorption capacity of oxygen-containing molecules [217]. A lower E_p relative to E_f indicates a higher ability of the catalyst to adsorb oxygen-containing species, which can enhance the electrocatalytic activity for reactions such as ORR and OER.

The ORR and OER processes generally involve the adsorption and activation of oxygen intermediates. The optimized adsorption configurations of reaction intermediates are crucial for enhancing the electrocatalytic performance of an electrocatalyst. For example, during the ORR, the adsorption of the OOH* and OH* intermediates on the surface of the catalyst are required to proceed through the four-electron pathway. In contrast, during OER, the adsorption of O* intermediate is necessary to proceed through the four-electron pathway [218]. Therefore, the optimized adsorption configurations of these intermediates

can strongly influence the electrocatalytic activity of the catalyst. The theoretical calculations for the variation in free energy (ΔG) related to the intermediates on active sites can be used to predict whether the reaction can proceed and the direction of the reaction. For example, Zheng et al. simulated the free energy diagrams of several models for ORR and OER. As shown in Fig. 12c, d, $Co_9S_8(311)@N$, S–C had the smallest barrier energy (0.503 eV) for ORR and the smallest barrier energy (0.571 eV) for the catalysis of OER among all the models, which explained its superior ORR and OER catalytic activity [199].

Orbital hybridization plays a key role in determining the reactivity and selectivity of electrocatalysts. Similar energy levels of the frontier orbitals of the catalyst and reactant facilitate the transfer of electrons, leading to efficient electrocatalysis. Yang et al. compared the lowest unoccupied orbital (LUMO) of $CaMnO_3$ (CMO), and distorted $CaMnO_3$ (D-CMO) and found that the oxygen has more orbital

contribution for D-CMO. The O orbitals of the OH* and O_2* adsorbates strongly interact with the surface of D-CMO, leading to a significant overlap and sharing of electrons. This σ-type electronic coupling indicates the formation of covalent bonds between the surface and the adsorbates, which can improve the catalytic activity of the material. The contribution of the O orbitals to the highest occupied orbital (HOMO) of the D-CMO further supports the presence of strong electronic coupling (Fig. 12e, f), which can improve the ORR and OER performance [159].

It should be noted that electrochemical systems are dynamic and exist in non-equilibrium states, which implies that theoretical simulations based on static surface models may not fully capture the complexity of the electrochemical reaction. Electrocatalysis of cathode catalysts occurs at the three-phase interface. A hydrophobic-aerophilic strategy has been devised to construct a self-supported air cathode utilizing CoS/Fe_3S_4 nanoparticles enclosed within S, N co-doped carbon plate arrays (CoS/Fe_3S_4@SNCP) to enhance the reaction kinetics at the air cathodes [146]. The finite element method (FEM) and ab initio molecular dynamics (AIMD) simulations were employed to delve deeper into the elucidation of the microenvironment origin for the catalysts. The FEM results indicate that the O_2 concentration at the hydrophobic CoS/Fe_3S_4@SNCP electrode (Fig. 12g) surpasses that at the hydrophilic CoS@SNCP electrode (Fig. 12h), implying that the enhanced hydrophobic and aerophilic properties of the CoS/Fe_3S_4@SNCP electrode can effectively expedite the diffusion of oxygen at the triple-phase interface. Furthermore, in representative structures from AIMD at 5.0 and 10.0 ps, as depicted in Fig. 12i, the formation of hydrophobic cavities emphasizes the hydrophobic nature of the CoS and CoS/Fe_3S_4 surfaces (indicated by the black shadow). This underscores that the observed formation of hydrophobic cavities through AIMD simulations and this comprehensive simulation approach offers crucial information about the microscopic mechanisms and dynamic processes governing the behavior of the catalysts. To more accurately reflect the chemical reactions occurring in these systems, more precise characterizations are necessary.

5.2 Data-Driven Machine Learning

Active machine learning (ML) methods has many applications in a range of reactions, helping to accelerate research in areas such as material design, prediction of reaction mechanisms, and performance optimization. Thus, ML methods enable the handling of larger systems with greater accuracy for ORR and OER. Li et al. developed an adaptive ML strategy to search for high-performance ABO_3-type cubic perovskites that can catalyze the OER. By learning the structure–reactivity relationships of approximately 250 initially computed perovskites, Li et al. developed an adaptive machine-learning strategy to analyze a larger set of double perovskites, including approximately 4000 $AA'B_2O_6$ double perovskites. Through this analysis, they identified about 10 stable cubic double perovskites with high OER catalytic activity. To identify these catalysts, they examined the feature distributions of the perovskites that were better or worse catalysts than $LaCoO_3$. Their findings suggested that the electronic structure of the metal B-site plays a key role in determining the OER activity of perovskite catalysts. Using this information, the design of new and more efficient catalysts can be determined. Data-driven models can be used to easily identify these underlying factors and gain a better understanding of the structure–activity relationships of these materials. This highlights the potential of machine learning approaches for accelerating the development of new materials and catalysts (Fig. 13a–c) [219]. To design highly efficient bifunctional electrocatalysts for ORR and OER, Liu et al. conducted a study and found that V_{Al}-$2N_P$-AlP (where two nitrogen atoms replace two P atoms with an Al vacancy) is the most optimal choice for anchoring metal atoms. The DFT results indicated that the Co@V_{Al}-$2N_P$-AlP and Ni@V_{Al}-$2N_P$-AlP systems exhibit a low overpotential for OER and ORR, making them promising candidates for application in ZABs. The ML method used in that study also showed that the number of TM-d electrons (N_e), the radius of the TM atom (r_d), and the charge transfer of TM atoms (Q_e) were the primary descriptors related to the adsorption behavior (Fig. 13d–f) [220].

The machine-learning method with large-scale simulations and massive experimental data is a new paradigm for discovering ideal catalysts, making it possible to conduct high-throughput science.
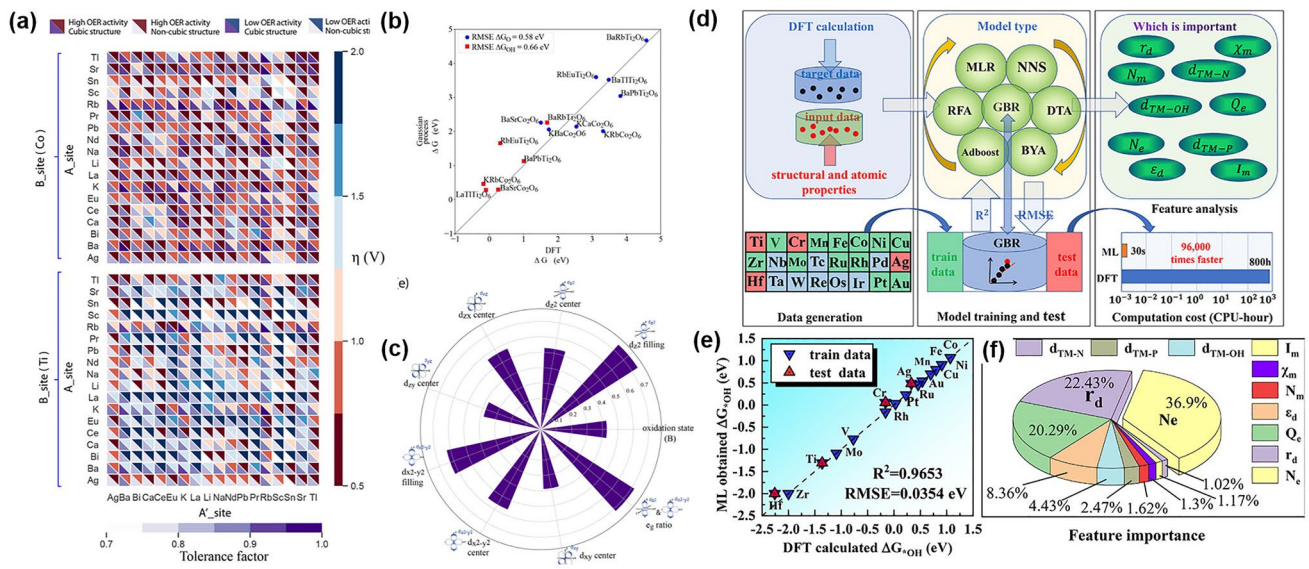
Fig. 13 **a** Heat map visualization of the OER activity of double perovskites as a function of A-site/B-site cations in terms of the OER overpotentials and cubic phase probability. The red/blue color bar represent the overpotentials, and the purple bar represents the tolerance factor. **b** Parity plot for DFT-calculated vs. Gaussian process model prediction of descriptor adsorption free energies on candidate perovskite structures. **c** Polar distribution plots of the most informatic descriptors (KL entropy index > 0.4). Reprinted with permission from Ref. [219]. **d** Brief description of the ML process, divided into three parts, the data from DFT calculation, the ML model, and the feature importance analysis. **e** Calculated DFT ΔG *OH vs. ΔG *OH value obtained from ML by the GBR algorithm. **f** Feature importance of each descriptor with the corresponding proportion. Reprinted with permission from Ref. [220]
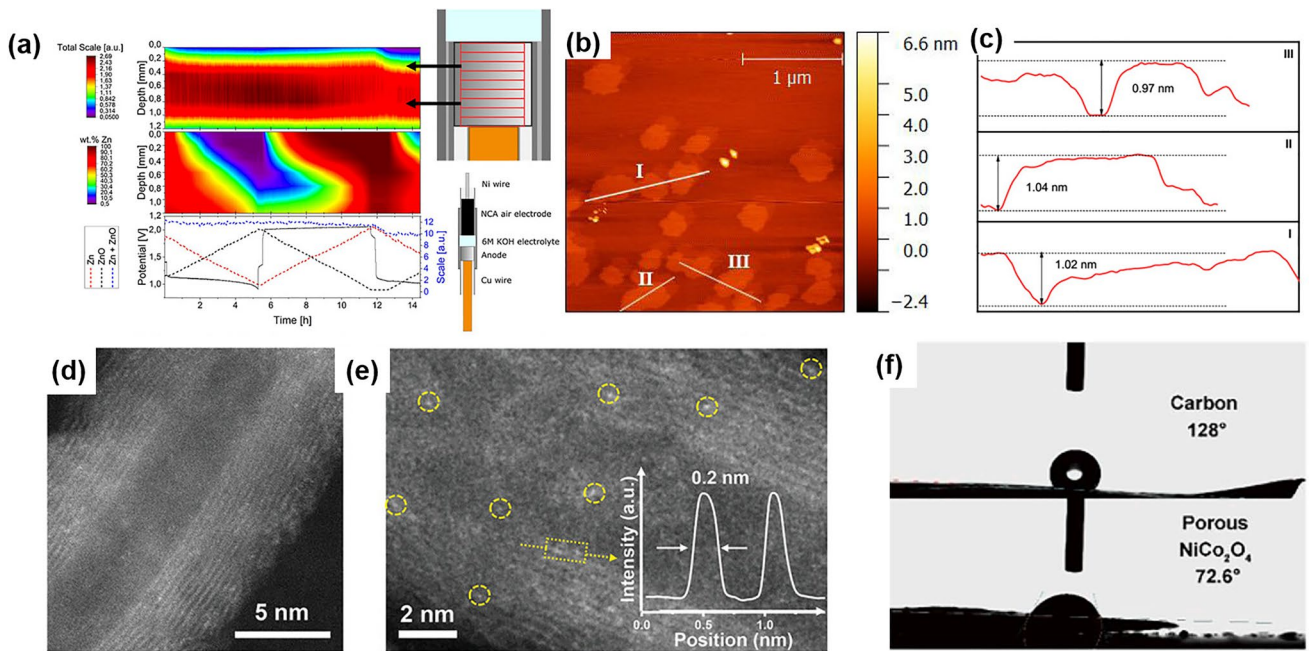

Fig. 14 **a** (Top) A heatmap of the summed scale factors for Zn and ZnO. (Middle) wt% Zn heatmap showing the reaction front of the Zn/ZnO phase transformation. (Bottom) voltage profile over time, shown with the corrected scale factor for Zn and ZnO. (Right) A close-up of the anode subdivided in 0.2 mm × 1 mm segments and schematic diagram showing the capillary-based ZAB. Reprinted with permission from Ref. [221]. **b** AFM image and **c** the corresponding height profiles of Cu/Fe-NG. Reprinted with permission from Ref. [82]. **d**, **e** HAADF-STEM image and corresponding EDS mapping images on N, Co, Ni, Fe, and O elements of CoNC@LDH. Reprinted with permission from Ref. [209]. **f** Comparative testing of the contact angles at air–water-solid catalyst interfaces. Reprinted with permission from Ref. [222]

5.3 Surface-Detection Techniques

While analyzing the electrochemical behavior of electrocatalysts in ZABs, their raw physiochemical properties and phase transformation in battery operation, as well as the corresponding changes in chemical composition and electrochemical performance, need to be determined. For this, advanced surface-detection techniques might provide useful information about electrified interfaces under operating conditions.

The commonly used methods for surface characterization include X-ray diffraction (XRD), XPS, scanning electron microscopy (SEM), and atomic force microscopy (AFM), among other techniques. XRD uses X-ray diffraction patterns to obtain information about the composition of materials, as well as the structure and morphology of atoms or molecules within the materials. Graae et al. used in-situ XRD to analyze the phase transition of the anode between pure Zn and ZnO (Fig. 14a). Their results indicated that the effectiveness of the air catalyst to run the reverse reaction was not the limiting factor for an effective secondary Zn-air cell; instead, the main challenge was the morphological changes in the anode over time, which limited the access to ZnO nucleation sites near the surface, thus increasing the overpotential required to initiate the discharge reaction [221]. XPS can be used to determine the elemental and chemical composition of surfaces and thin films. It can also provide semi-quantitative information on the elemental composition of the sample surface by measuring the peak intensity of the XPS peaks. However, XPS is a surface-sensitive technique and can only provide information about the top few nanometers of the sample surface.

Scanning probe microscope (SPM) is a new microscope tool with several advantages over other types of microscopes and analytical instruments. SPM can provide high-resolution data. It can readily "see" atoms in a way that cannot be achieved via ordinary electron microscopes. In recent studies, many atom-thick nanosheets were characterized by SPM for analyzing their surface structure and physical thickness. For example, Li et al. studied exfoliation-derived metallic $CuCo_2S_4$ nanosheets with an atom-thick layer using an atomic force microscope (AFM; one type of SPM). The height of $CuCo_2S_4$ nanosheets was found to be 0.90–1.25 nm, reflecting a thickness of 4–6 atomic layers [189]. The results suggested that the ultrathin nanosheet structure of $CuCo_2S_4$ NSs provided exposed active sites,

resulting in excellent electrocatalytic performance. Xu et al. reported the synthesis of Cu nanoclusters/FeN_4 amorphous composites embedded in N-doped graphene (Cu/Fe–NG). They used AFM to observe its surface texture and thickness. In a 2 μm × 3 μm field of view, homogeneous contrast verified the uniform smooth surface of graphene. The corresponding height profiles revealed that Cu/Fe-NG had a thickness of 0.35–1.05 nm, indicating the presence of 1–3 stacked layers (Fig. 14b, c) [82]. High electrocatalytic performance was associated with the benefits of 2D nanostructures with atomic thickness, which increased the surficial active site ratio, improved the contact interfacial area, and decreased surface energy.

The dynamic interplay of the ORR and OER at triple-phase boundaries underscores the importance of optimizing surface hydrophilic/aerophilic properties, particularly within a static environment. Recognizing this critical aspect, an investigation into the contact angles on different catalysts was undertaken using a high-speed camera, as illustrated in Fig. 14f [222]. Notably, the porous $NiCo_2O_4$ catalyst exhibited a water–solid-air interface angle of 72.6°, in stark contrast to the 128° observed on the carbon surface. This distinction emphasizes the desirable hydrophilic nature of porous $NiCo_2O_4$, strategically balancing the contracting forces between gases and aqueous electrolyte.

5.4 Atomic Scale Characterization

Atomic scale characterization methods can be used to elucidate the structure and properties of materials at the atomic level. Various methods can be used to characterize the atomic structure of materials, including Scanning Tunneling Microscopy (STM), Transmission Electron Microscopy (TEM), Raman, X-ray absorption spectroscopy, etc.

Aberration-corrected scanning transmission electron microscopy (AC-STEM) can be used to obtain atomic-resolution images at a low-order zone axis orientation. AC-STEM can distinguish the spatial atomic distribution and directly show the distribution and defective properties, as well as, disordered local symmetry. Zhao et al. used high-angle annular dark field scanning transmission electron microscopy (HAADF-STEM; a type of AC-STEM) to visualize single-atom Co inside the LDH, where the bright dots were resolved as Co atoms (Fig. 14d, e) [209].

Meng et al. reported another example regarding the spatial isolation of Fe species at the atomic scale by regulating the content of Co nanoparticles in MOF-derived carbon. This allowed for the preparation of nanoparticles, atomic clusters, and single-atom Fe catalysts on N-doped porous carbon [90]. The prepared Co nanoparticles and highly dispersed Fe loaded on N-doped carbon can provide ZABs with excellent bifunctional activity and durability. More intriguingly, the vacancy defects and rearrangement can also be observed by TEM. However, AC-STEM has difficulty distinguishing between elements with similar atomic numbers. Additionally, the coordination species, such as metal–carbon and metal–metal bonds, cannot be identified by AC-STEM.

Raman spectroscopy is often combined with infrared testing as they complement each other. By assessing the Raman frequency, the substance can be identified, and its quality can be determined. Raman displacement changes correspond to material stress, tension, and doping, while peak strength can be semi-quantified for the substance. Changes in the peak width can indicate disorder and defects in the substance. Liu

et al. used in situ Raman spectroscopy to elucidate the catalytic mechanism of CoNi catalysts for ORR and OER. During the ORR, the peaks showed the conversion of Co(III)/Ni(III) to Co(II)/Ni(II), while the OER process showed the opposite pattern, suggesting that the ORR and OER on CoNi catalysts occurred through the reduction and oxidation of M(II) and M(III) species (Fig. 15a, b) [223]. Furthermore, the electrocatalysts exhibiting microstructural changes and defects can be identified using Raman spectroscopy. This method allows for the real-time detection of alterations in chemical bonds.

Synchrotron-based X-ray absorption spectroscopy (XAS) is a new and powerful technique that can be used for characterizing the geometric structure of active sites in electrocatalysts. This technique can be divided into two energy regions, including the X-ray absorption near-edge structure (XANES) and the extended X-ray absorption fine-structure (EXAFS). XANES is highly sensitive to the oxidation states and the coordination structure, such as whether the metal species are in tetrahedral or octahedral sites. On the other hand, EXAFS is used to evaluate the
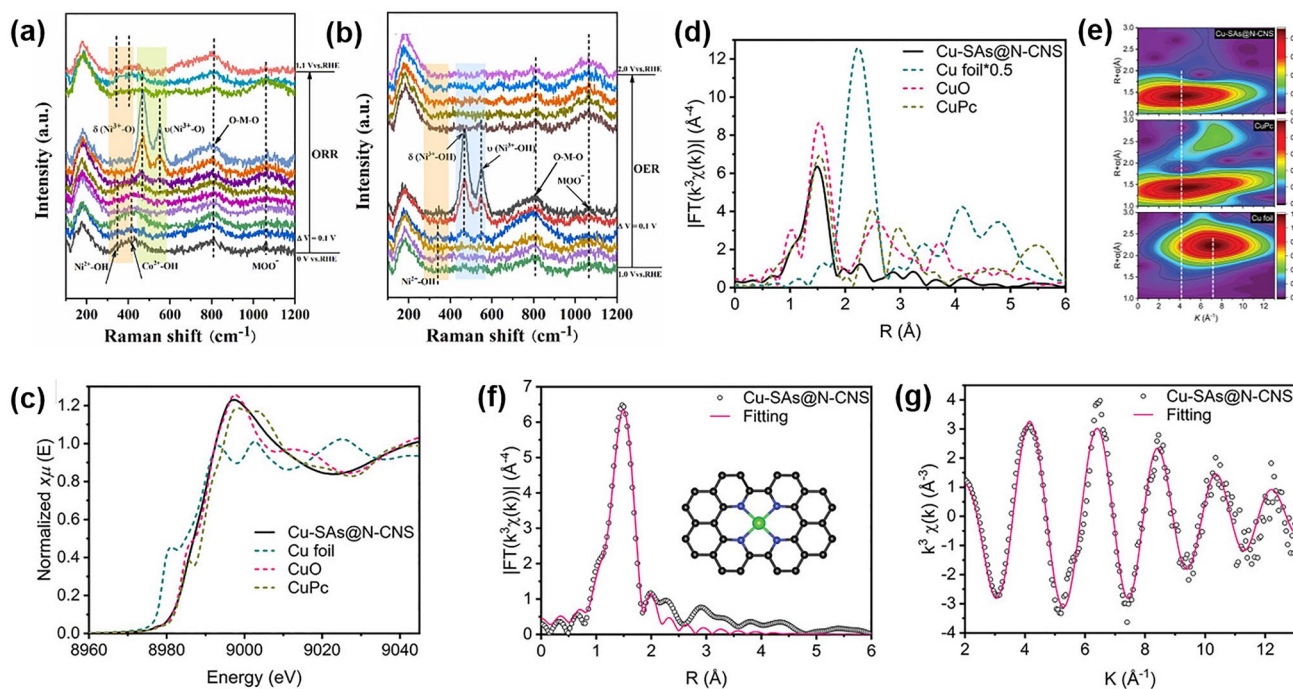

Fig. 15 In situ Raman spectra collected on CoNi-CoN$_4$-HPC-900 for **a** the ORR process and **b** the OER process in 0.1 M KOH solution. Reprinted with permission from Ref. [223]. **c** Cu K-edge XANES, **d** FT k^3-weighted Cu K-edge EXAFS, and **e** WT-EXAFS spectra of Cu-SAs@N-CNS and Reference samples. **f, g** FT-EXAFS fitting curves for Cu-SAs@N-CNS in R and K spaces. Reprinted with permission from Ref. [211]

local coordination and bonding environment of metal atoms. These two regions of XAS provide valuable information about the electronic and geometric structures of active sites in electrocatalysts [224]. For example, Zong et al. prepared Cu single atoms anchored to carbon (Cu-SAs@N-CNS). The valence state of Cu was found to be close to $+2$ by XANES analysis, and the Fourier transformation of EXAFS results showed the existence of Cu-N_x coordination, where the x number was 4.1 (Fig. 15c–e). The Morlet wavelet transform (MWT) is a powerful technique for analyzing the local environment of metal complexes by directly visualizing multiple scattering signals from neighboring atoms in the EXAFS spectra. This technique can be used to effectively extract information about the geometric structure of metal complexes by analyzing the oscillations in the EXAFS spectra at different frequencies. The quantitative least-squares EXAFS curve-fitting analysis plot of Cu-SAs@N-CNS (Fig. 15f, g) showed a single contour peak with a maximum intensity at 4.2 $Å^{-1}$, which was close to that of CuPc with Cu-N_4 bonds. This suggested the presence of a Cu–N_x coordination configuration in Cu-SAs@N-CNS [211]. Zhang et al. introduced Mg into a three-dimensional ordered mesoporous material (denoted as 3DOM $Mg_xCo_{3-x}O_4$). In the XANES spectra, the shift of 3DOM $Mg_xCo_{3-x}O_4$ was consistent with that of MgO, indicating that the valence state of Mg was $+2$. The contour plots of the EXAFS wavelet transforms for 3DOM $Mg_xCo_{3-x}O_4$ and pristine Co_3O_4 confirmed the chemical coordination of Co–Co and Co–O, indicating that the inclusion of Mg in Co_3O_4 can modulate the electronic structure of 3DOM $Mg_xCo_{3-x}O_4$ and enhance its intrinsic catalytic performance during charge and discharge processes [225]. Zheng et al. synthesized sulfur-doped NiCo-(oxy)hydroxysulfides. The results of the Morlet wavelet transform confirmed that the incorporation of S in the composites can effectively regulate the local environment and the electronic structure of the metallic sites, leading to enhanced catalytic activity and stability when used as anodes in Zn-air batteries [226].

Positron annihilation spectroscopy (PAS) is a technique used in materials science to study the properties of materials at the atomic and molecular levels. This method involves the interaction of positrons, which are positively charged antiparticles of electrons, with electrons in a material. PAS is widely acknowledged as a highly appropriate method for characterizing open volume defects [227]. The positron lifetime is subject to variation depending on the electron density surrounding the positron. Consequently, when positrons annihilate from defects, their lifetime is extended compared to that in defect-free materials. This distinction allows for the identification of potential defects through positron annihilation lifetime spectroscopy (PALS), wherein the extracted lifetime components serve as indicators of these defects [228]. Electron Spin Resonance (ESR), also known as Electron Paramagnetic Resonance (EPR), is a spectroscopic technique that investigates the interaction between unpaired electrons and an external magnetic field. In addition to PALS, electron spin resonance (ESR) can also be employed to characterize the degree of defects in materials.

5.5 Characterization Under Operating Conditions

To explore the reversibility of the zinc–air battery and the specific role played by the bifunctional electrocatalysts, characterization is required to capture the structural and chemical transformation under battery-operating conditions, which is different from the common half-cell (namely three electrodes system: working electrode, reference electrode, counter electrode). The operational context is of utmost importance. Zheng et al. have innovatively incorporated thermoelectric devices and materials, seamlessly integrating the thermoelectric system with zinc–air batteries. This integration has resulted in a substantial improvement in the energy efficiency of ZABs [229]. The ZAB prototype with flowing electrolyte could eliminate electrolyte-induced performance variation to allow direct focus on the behavior of bifunctional electrocatalysts under operating conditions. Sun et al. designed an operando synchrotron radiation infrared spectroscopy (SRIR) device to investigate the realistic battery-operating conditions (Fig. 16a). The device facilitated the mass transport of O_2 during ORR, which was different from the conventional half-reaction cell used in many studies [230]. Deng et al. investigate the evolution of Co species during the charge and discharge process in Zn-air batteries by in situ XRD and XAS. The Co K-edge XANES results showed that the valence state of Co continued to increase during the process, as shown in Fig. 16b, c. A dynamic illustration depicting the formation and development of a nanoscale oxyhydroxide shell is provided, with periodic shifts in the valence state of the performance-dominant element being observed [192]. The operando XAS and SRIR
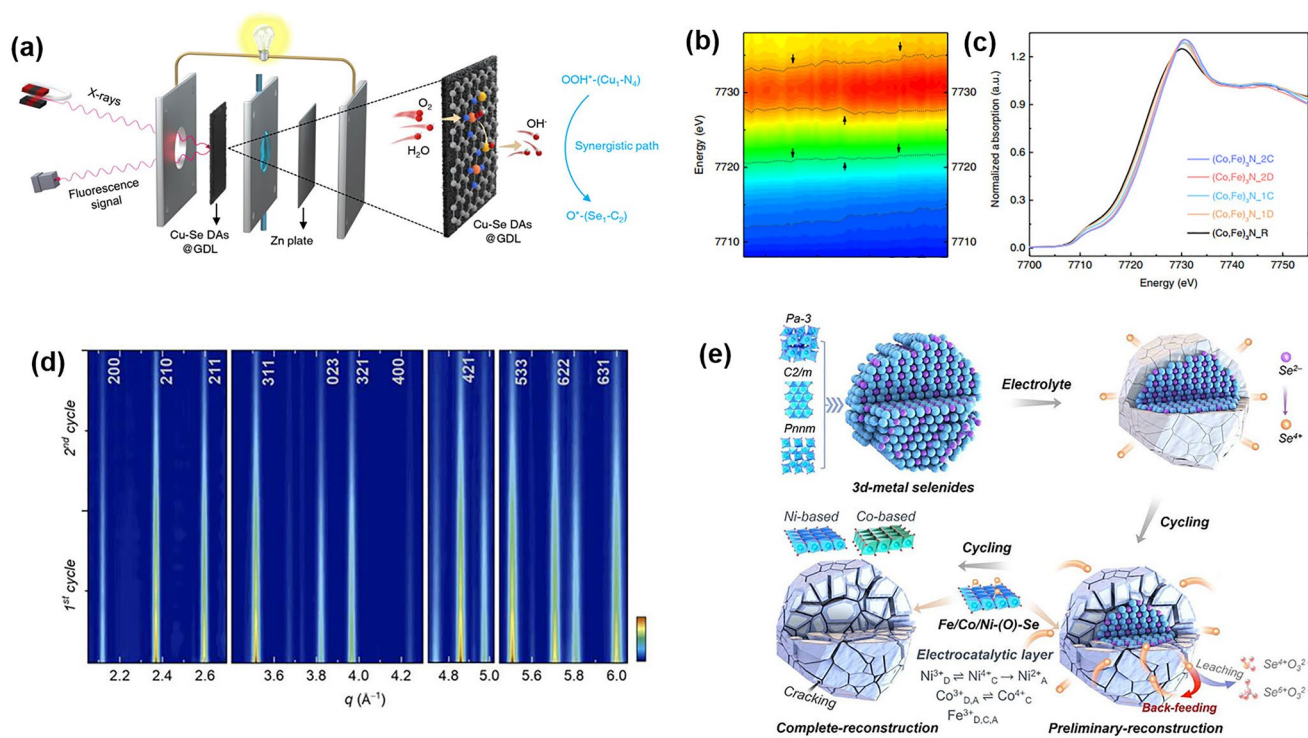
Fig. 16 **a** Illustration of operando XAS set up for ZAB under realistic device working conditions. Reprinted with permission from Ref. [230]. **b**, **c** The operando XANES spectra of Co. Reprinted with permission from Ref. [192]. **d** Operando 2D HEXRD contour map of (Fe, Ni)Se$_2$ in a Zn–air battery. **e** Schematic demonstration of the Se-driven reconstruction mechanism. Reprinted with permission from Ref. [231]

device provided valuable insights into the mechanism of Zn-air batteries by allowing for the in-depth investigation of the electrochemical and spectroscopic properties of the catalyst under realistic conditions. Recently, an electrolyte-induced layer-by-layer ZAB is employed to eliminate performance variation with operando HEXRD (Fig. 16d, e), suggesting the reconstructed phase during the stages of charge and discharge [231]. The procedure results in the formation of an amorphous (oxy)hydroxide featuring selenium motifs with shared oxygen bonds. This, in turn, initiates charge redistribution at metal sites, reducing the energetic barrier for their current-driven redox processes.

Researchers agree that oxygen electrocatalysis is a dynamic process. However, different electrocatalysts may experience different self-reconstruction processes during the cycling of ZABs, and it's difficult to visualize accurately. In-situ characterizations, such as XRD, Raman, and XAS, provide accurate information on the surface structure, including changes in the local coordination environment,

structure, and oxidation state of electrocatalysts during battery cycling. By using in situ detection techniques, distinct changes in the composition and structure of the electrocatalyst can be probed. During the reaction, operando detection can be further utilized to monitor the catalytic intermediates and microenvironments. The in situ techniques provide a reliable basis for conducting theoretical and experimental studies for screening catalytic systems.

6 Summary and Outlook

High-performance zinc–air batteries represent a promising technology for next-generation rechargeable batteries, and efficient electrocatalysts are the key to advancing these batteries from the laboratory to the industry. In this review, we provided an overview of the mainstream methods used for fabricating non-noble-metal electrocatalysts for ORR/OER. Recent advancements in understanding catalyst engineering and elucidating the reaction mechanisms were made using

theoretical calculations and advanced techniques. However, further investigation is necessary to perfect this field.

(1) Although many high-performance ORR and OER catalysts have been developed over the past few years, researchers have failed to determine a universal structure–activity/selectivity relationship to guide catalyst design. The most frequently used strategies to develop an ideal catalyst involve optimizing the number of active sites and the intrinsic activity of each active site. Here, we outlined the principles of catalyst design in four major aspects, including morphology, crystal structure, interface, and atomic engineering. Most of these principles can be deduced from experimental results and computational simulations. Therefore, future studies need to determine the true structure-performance relationship and provide predictive guidelines for designing bifunctional catalysts for ORR and OER with optimized activity and durability.

(2) Gas-solid-liquid triple-phase reactions at the cathode strongly influence the performance of ZABs. Identifying appropriate catalysts can help in the synergistic optimization of electron conduction, oxygen gas diffusion, and ion transport for electrocatalysis, which in turn can accelerate the understanding of the reaction mechanism at the triple-phase interface.

(3) During battery operation, the performance of air-electrodes is degraded due to carbon corrosion/oxidation at oxidation potential in high-concentrated alkaline electrolyte. This inferior stability and cyclability greatly shorten the operation lifetime of ZABs. To minimize and further eliminate the employment of carbon might be one possible solution. Attempts to replace carbon with highly conductive metal-based substrates (such as carbides) have shown some interesting results. Although metal-based batteries have a satisfactory lifetime, their bifunctional activity cannot compete with that of carbon-based batteries, as carbon is also an excellent electrocatalyst besides the substrate. Therefore, highly active and conductive metal-based electrocatalysts need to be identified for long-lasting ZABs.

(4) The evolution of most bifunctional electrocatalysts is still unclear due to the lack of theoretical prediction and in situ characterizations. To solve this problem, advanced operando characterization techniques, theoretical computations, and machine learning methods can be used together to achieve a fundamental understanding of the electrochemical behavior of electrocatalysts in ZABs. By using this strategy, vital information

might be revealed that might be used as the design principles for further material development.

(5) Most electrocatalysts are prepared in a highly controlled environment and at a laboratory scale, and thus, their application shows poor reproducibility at the industrial scale. Additionally, electrocatalysts with nanostructures are sensitive to electrochemical measurements, and their rechargeability cannot meet large-scale requirements. Thus, to meet the demands of industrial applications, inexpensive, easy-to-synthesize, and stable catalysts need to be developed.

Declarations

References

1. H. Hafiz, K. Suzuki, B. Barbiellini, N. Tsuji, N. Yabuuchi et al., Tomographic reconstruction of oxygen orbitals in lithium-rich battery materials. Nature **594**, 213–216 (2021). https://doi.org/10.1038/s41586-021-03509-z

2. Z. Dai, S.K. Yadavalli, M. Chen, A. Abbaspourtamijani, Y. Qi et al., Interfacial toughening with self-assembled monolayers enhances perovskite solar cell reliability. Science **372**, 618–622 (2021). https://doi.org/10.1126/science.abf5602

3. J. Li, W. Zhou, D. Zhu, J. He, C. Wu et al., Ni_3S_2-coated metal hydride anode with high-power and long-life performance for low-temperature Ni-MH power batteries. Chem. Eng. J. **379**, 122204 (2020). https://doi.org/10.1016/j.cej.2019.122204

4. D.A. Kitchaev, J. Vinckeviciute, A. Van der Ven, Delocalized metal-oxygen π-redox is the origin of anomalous nonhysteretic capacity in Li-ion and Na-ion cathode materials. J. Am. Chem. Soc. **143**, 1908–1916 (2021). https://doi.org/10.1021/jacs.0c10704

5. R. Feng, X. Zhang, V. Murugesan, A. Hollas, Y. Chen et al., Reversible ketone hydrogenation and dehydrogenation for aqueous organic redox flow batteries. Science **372**, 836–840 (2021). https://doi.org/10.1126/science.abd9795

6. A. Singh, P.B. Karandikar, N.R. Kulkarni, Mitigation of sulfation in lead acid battery towards life time extension using ultra capacitor in hybrid electric vehicle. J. Energy Storage **34**, 102219 (2021). https://doi.org/10.1016/j.est.2020.102219

7. H.-H. Ryu, H.H. Sun, S.-T. Myung, C.S. Yoon, Y.-K. Sun, Reducing cobalt from lithium-ion batteries for the electric vehicle era. Energy Environ. Sci. **14**, 844–852 (2021). https://doi.org/10.1039/D0EE03581E

8. S. Ko, Y. Yamada, A. Yamada, An overlooked issue for high-voltage Li-ion batteries: suppressing the intercalation of anions into conductive carbon. Joule **5**, 998–1009 (2021). https://doi.org/10.1016/j.joule.2021.02.016

9. F. Wang, B. Wang, J. Li, B. Wang, Y. Zhou et al., Prelithiation: a crucial strategy for boosting the practical application of next-generation lithium ion battery. ACS Nano **15**, 2197–2218 (2021). https://doi.org/10.1021/acsnano.0c10664

10. S. Yin, W. Deng, J. Chen, X. Gao, G. Zou et al., Fundamental and solutions of microcrack in Ni-rich layered oxide cathode materials of lithium-ion batteries. Nano Energy **83**, 105854 (2021). https://doi.org/10.1016/j.nanoen.2021.105854

11. X. Shen, Q. Zhou, M. Han, X. Qi, B. Li et al., Rapid mechanochemical synthesis of polyanionic cathode with improved electrochemical performance for Na-ion batteries. Nat. Commun. **12**, 2848 (2021). https://doi.org/10.1038/s41467-021-23132-w

12. X. Min, J. Xiao, M. Fang, W.A. Wang, Y. Zhao et al., Potassium-ion batteries: outlook on present and future technologies. Energy Environ. Sci. **14**, 2186–2243 (2021). https://doi.org/10.1039/d0ee02917C

13. J. Zhou, Y. Yang, Y. Zhang, S. Duan, X. Zhou et al., Sulfur in amorphous silica for an advanced room-temperature sodium–sulfur battery. Angew. Chem. Int. Ed. **60**, 10129–10136 (2021). https://doi.org/10.1002/anie.202015932

14. D. Luo, L. Zheng, Z. Zhang, M. Li, Z. Chen et al., Constructing multifunctional solid electrolyte interface via in situ polymerization for dendrite-free and low N/P ratio lithium metal batteries. Nat. Commun. **12**, 186 (2021). https://doi.org/10.1038/s41467-020-20339-1

15. Z. Yuan, L. Wang, D. Li, J. Cao, W. Han, Carbon-reinforced Nb_2CT_x MXene/MoS_2 nanosheets as a superior rate and high-capacity anode for sodium–ion batteries. ACS Nano **15**, 7439–7450 (2021). https://doi.org/10.1021/acsnano.1c00849

16. Q. Li, H. Wang, X. Tang, M. Zhou, H. Zhao et al., Electrical conductivity adjustment for interface capacitive-like storage in sodium–ion battery. Adv. Funct. Mater. **31**, 2101081 (2021). https://doi.org/10.1002/adfm.202101081

17. B. Xie, L. Wang, H. Li, H. Huo, C. Cui et al., An interface-reinforced rhombohedral Prussian blue analogue in semi-solid state electrolyte for sodium–ion battery. Energy Storage Mater. **36**, 99–107 (2021). https://doi.org/10.1016/j.ensm.2020.12.008

18. M. Li, J. Lu, J. Shi, S.-B. Son, D. Luo et al., In situ localized polysulfide injector for the activation of bulk lithium sulfide. J. Am. Chem. Soc. **143**, 2185–2189 (2021). https://doi.org/10.1021/jacs.0c11265

19. M. Zhao, H.-J. Peng, B.-Q. Li, X. Chen, J. Xie et al., Electrochemical phase evolution of metal-based pre-catalysts for high-rate polysulfide conversion. Angew. Chem. Int. Ed. **59**, 9011–9017 (2020). https://doi.org/10.1002/anie.202003136

20. L. Sharma, R. Gond, B. Senthilkumar, A. Roy, P. Barpanda, Fluorophosphates as efficient bifunctional electrocatalysts for metal–air batteries. ACS Catal. **10**, 43–50 (2020). https://doi.org/10.1021/acscatal.9b03686

21. B. He, G. Li, J. Li, J. Wang, H. Tong et al., $MoSe_2$@CNT core–shell nanostructures as grain promoters featuring a direct Li_2O_2 formation/decomposition catalytic capability in lithium–oxygen batteries. Adv. Energy Mater. **11**, 2003263 (2021). https://doi.org/10.1002/aenm.202003263

22. X. Lin, Y. Sun, Q. Sun, J. Luo, Y. Zhao et al., Reviving anode protection layer in Na–O_2 batteries: failure mechanism and resolving strategy. Adv. Energy Mater. **11**, 2003789 (2021). https://doi.org/10.1002/aenm.202003789

23. W. Wang, Y. Wang, C.-H. Wang, Y.-W. Yang, Y.-C. Lu, In Situ probing of solid/liquid interfaces of potassium–oxygen batteries via ambient pressure X-ray photoelectron spectroscopy: new reaction pathways and root cause of battery degradation. Energy Storage Mater. **36**, 341–346 (2021). https://doi.org/10.1016/j.ensm.2021.01.010

24. Y. Jiang, Y.-P. Deng, R. Liang, J. Fu, R. Gao et al., D-orbital steered active sites through ligand editing on heterometal imidazole frameworks for rechargeable zinc–air battery. Nat. Commun. **11**, 5858 (2020). https://doi.org/10.1038/s41467-020-19709-6

25. L. Li, H. Chen, E. He, L. Wang, T. Ye et al., High-energy-density magnesium-air battery based on dual-layer gel electrolyte. Angew. Chem. Int. Ed. **60**, 15317–15322 (2021). https://doi.org/10.1002/anie.202104536

26. X. Fu, G. Jiang, G. Wen, R. Gao, S. Li et al., Densely accessible Fe–N_x active sites decorated mesoporous-carbon-spheres for oxygen reduction towards high performance aluminum-air flow batteries. Appl. Catal. B Environ. **293**, 120176 (2021). https://doi.org/10.1016/j.apcatb.2021.120176

27. M.A. Deyab, Q. Mohsen, Improved battery capacity and cycle life in iron-air batteries with ionic liquid. Renew. Sustain. Energy Rev. **139**, 110729 (2021). https://doi.org/10.1016/j.rser.2021.110729

28. C. Wei, Y. Zhang, Y. Tian, L. Tan, Y. An et al., Design of safe, long-cycling and high-energy lithium metal anodes in

all working conditions: progress, challenges and perspectives. Energy Storage Mater. **38**, 157–189 (2021). https://doi.org/10.1016/j.ensm.2021.03.006

29. Q. Liu, R. Liu, C. He, C. Xia, W. Guo et al., Advanced polymer-based electrolytes in zinc–air batteries. eScience **2**, 453–466 (2022). https://doi.org/10.1016/j.esci.2022.08.004

30. S. Zhang, Y. Liu, Q. Fan, C. Zhang, T. Zhou et al., Liquid metal batteries for future energy storage. Energy Environ. Sci. **14**, 4177–4202 (2021). https://doi.org/10.1039/D1EE00531F

31. L. Wang, D. Snihirova, M. Deng, B. Vaghefinazari, W. Xu et al., Sustainable aqueous metal-air batteries: an insight into electrolyte system. Energy Storage Mater. **52**, 573–597 (2022). https://doi.org/10.1016/j.ensm.2022.08.032

32. Q. Tang, Y. Zhang, N. Xu, X. Lei, K. Huang, Demonstration of 10+ hour energy storage with ϕ1″ laboratory size solid oxide iron–air batteries. Energy Environ. Sci. **15**, 4659–4671 (2022). https://doi.org/10.1039/D2EE01626E

33. S. Song, W. Li, Y.-P. Deng, Y. Ruan, Y. Zhang et al., TiC supported amorphous MnO_x as highly efficient bifunctional electrocatalyst for corrosion resistant oxygen electrode of Zn–air batteries. Nano Energy **67**, 104208 (2020). https://doi.org/10.1016/j.nanoen.2019.104208

34. M.-H. Lin, C.-J. Huang, P.-H. Cheng, J.-H. Cheng, C.-C. Wang, Revealing the effect of polyethylenimine on zinc metal anodes in alkaline electrolyte solution for zinc–air batteries: mechanism studies of dendrite suppression and corrosion inhibition. J. Mater. Chem. A **8**, 20637–20649 (2020). https://doi.org/10.1039/D0TA06929A

35. R. Khezri, S. Rezaei Motlagh, M. Etesami, A.A. Mohamad, F. Mahlendorf et al., Stabilizing zinc anodes for different configurations of rechargeable zinc–air batteries. Chem. Eng. J. **449**, 137796 (2022). https://doi.org/10.1016/j.cej.2022.137796

36. D. Stock, S. Dongmo, J. Janek, D. Schröder, Benchmarking anode concepts: the future of electrically rechargeable zinc–air batteries. ACS Energy Lett. **4**, 1287–1300 (2019). https://doi.org/10.1021/acsenergylett.9b00510

37. X. Wang, J. Sunarso, Q. Lu, Z. Zhou, J. Dai et al., High-performance platinum-perovskite composite bifunctional oxygen electrocatalyst for rechargeable Zn–air battery. Adv. Energy Mater. **10**, 1903271 (2020). https://doi.org/10.1002/aenm.201903271

38. L. Yang, X. Zeng, D. Wang, D. Cao, Biomass-derived FeNi alloy and nitrogen-codoped porous carbons as highly efficient oxygen reduction and evolution bifunctional electrocatalysts for rechargeable Zn–air battery. Energy Storage Mater. **12**, 277–283 (2018). https://doi.org/10.1016/j.ensm.2018.02.011

39. H. Liu, R. Xie, Z. Niu, Q. Jia, L. Yang et al., Two-in-one strategy to construct bifunctional oxygen electrocatalysts for rechargeable Zn–air battery. Chin. J. Catal. **43**, 2906–2912 (2022). https://doi.org/10.1016/S1872-2067(21)63979-7

40. M. Luo, W. Sun, B.B. Xu, H. Pan, Y. Jiang, Interface engineering of air electrocatalysts for rechargeable zinc–air batteries. Adv. Energy Mater. **11**, 2002762 (2021). https://doi.org/10.1002/aenm.202002762

41. T. Zhou, N. Zhang, C. Wu, Y. Xie, Surface/interface nanoengineering for rechargeable Zn–air batteries. Energy Environ. Sci. **13**, 1132–1153 (2020). https://doi.org/10.1039/C9EE03634B

42. F. Dong, M. Wu, Z. Chen, X. Liu, G. Zhang et al., Atomically dispersed transition metal-nitrogen-carbon bifunctional oxygen electrocatalysts for zinc–air batteries: recent advances and future perspectives. Nano-Micro Lett. **14**, 36 (2021). https://doi.org/10.1007/s40820-021-00768-3

43. B. Scrosati, History of lithium batteries. J. Solid State Electrochem. **15**, 1623–1630 (2011). https://doi.org/10.1007/s10008-011-1386-8

44. G.W. Heise, E.A. Schumacher, C.R. Fisher, The air-depolarized primary cell with caustic alkali electrolyte II. Trans. Electrochem. Soc. **92**, 173 (1947). https://doi.org/10.1149/1.3071813

45. H. Liu, X.-B. Cheng, J.-Q. Huang, H. Yuan, Y. Lu et al., Controlling dendrite growth in solid-state electrolytes. ACS Energy Lett. **5**, 833–843 (2020). https://doi.org/10.1021/acsenergylett.9b02660

46. Z. Chen, A. Yu, D. Higgins, H. Li, H. Wang et al., Highly active and durable core-corona structured bifunctional catalyst for rechargeable metal-air battery application. Nano Lett. **12**, 1946–1952 (2012). https://doi.org/10.1021/nl2044327

47. Y. Li, M. Gong, Y. Liang, J. Feng, J.-E. Kim et al., Advanced zinc-air batteries based on high-performance hybrid electrocatalysts. Nat. Commun. **4**, 1805 (2013). https://doi.org/10.1038/ncomms2812

48. J. Fu, F.M. Hassan, J. Li, D.U. Lee, A.R. Ghannoum et al., Flexible rechargeable zinc-air batteries through morphological emulation of human hair array. Adv. Mater. **28**, 6421–6428 (2016). https://doi.org/10.1002/adma.201600762

49. T. Zhou, H. Shan, H. Yu, C.-A. Zhong, J. Ge et al., Nanopore confinement of electrocatalysts optimizing triple transport for an ultrahigh-power-density zinc–air fuel cell with robust stability. Adv. Mater. **32**, e2003251 (2020). https://doi.org/10.1002/adma.202003251

50. W. Sun, F. Wang, B. Zhang, M. Zhang, V. Küpers et al., A rechargeable zinc-air battery based on zinc peroxide chemistry. Science **371**, 46–51 (2021). https://doi.org/10.1126/science.abb9554

51. Y. Gong, B. Wang, H. Ren, D. Li, D. Wang et al., Recent advances in structural optimization and surface modification on current collectors for high-performance zinc anode: principles, strategies, and challenges. Nano-Micro Lett. **15**, 208 (2023). https://doi.org/10.1007/s40820-023-01177-4

52. J.H. Park, C.H. Lee, J.-M. Ju, J.-H. Lee, J. Seol et al., Bifunctional covalent organic framework-derived electrocatalysts with modulated *p*-band centers for rechargeable Zn–air batteries. Adv. Funct. Mater. **31**, 2101727 (2021). https://doi.org/10.1002/adfm.202101727

53. Z. Sun, Y. Wang, L. Zhang, H. Wu, Y. Jin et al., Simultaneously realizing rapid electron transfer and mass transport in jellyfish-like mott–schottky nanoreactors for oxygen reduction reaction. Adv. Funct. Mater. **30**, 1910482 (2020). https://doi.org/10.1002/adfm.201910482

54. A.K. Worku, D.W. Ayele, N.G. Habtu, Recent advances and future perspectives in engineering of bifunctional electrocatalysts for rechargeable zinc–air batteries. Mater. Today Adv. **9**, 100116 (2021). https://doi.org/10.1016/j.mtadv.2020.100116

55. F. Pan, Z. Li, Z. Yang, Q. Ma, M. Wang et al., Porous FeCo glassy alloy as bifunctional support for high-performance Zn–air battery. Adv. Energy Mater. **11**, 2002204 (2021). https://doi.org/10.1002/aenm.202002204

56. C.-Y. Chen, K. Matsumoto, K. Kubota, R. Hagiwara, Q. Xu, A room-temperature molten hydrate electrolyte for rechargeable zinc–air batteries. Adv. Energy Mater. **9**, 1900196 (2019). https://doi.org/10.1002/aenm.201900196

57. Q. Liu, Z. Pan, E. Wang, L. An, G. Sun, Aqueous metal-air batteries: fundamentals and applications. Energy Storage Mater. **27**, 478–505 (2020). https://doi.org/10.1016/j.ensm.2019.12.011

58. L. Long, H. Liu, J. Jia, Y. Zhang, S. Dong, $Co_{0.7}Fe_{0.3}$ NPs confined in yolk–shell N-doped carbon: engineering multi-beaded fibers as an efficient bifunctional electrocatalyst for Zn–air batteries. Nanoscale **13**, 2609–2617 (2021). https://doi.org/10.1039/D0NR08781E

59. X. Zheng, X. Cao, K. Zeng, J. Yan, Z. Sun et al., A self-jet vapor-phase growth of 3D FeNi@NCNT clusters as efficient oxygen electrocatalysts for zinc–air batteries. Small **17**, e2006183 (2021). https://doi.org/10.1002/smll.202006183

60. H. Zhang, M. Zhao, H. Liu, S. Shi, Z. Wang et al., Ultrastable FeCo bifunctional electrocatalyst on Se-doped CNTs for liquid and flexible all-solid-state rechargeable Zn–air batteries. Nano Lett. **21**, 2255–2264 (2021). https://doi.org/10.1021/acs.nanolett.1c00077

61. C. Ma, Y. Feng, X. Liu, Y. Yang, L. Zhou et al., Dual-engineered separator for highly robust, all-climate lithium-sulfur batteries. Energy Storage Mater. **32**, 46–54 (2020). https://doi.org/10.1016/j.ensm.2020.07.034

62. X.F. Lu, S.L. Zhang, E. Shangguan, P. Zhang, S. Gao et al., Nitrogen-doped cobalt pyrite yolk-shell hollow spheres for long-life rechargeable Zn–air batteries. Adv. Sci. **7**, 2001178 (2020). https://doi.org/10.1002/advs.202001178

63. Y. Tian, X. Liu, L. Xu, D. Yuan, Y. Dou et al., Engineering crystallinity and oxygen vacancies of Co(II) oxide nanosheets for high performance and robust rechargeable Zn–air batteries. Adv. Funct. Mater. **31**, 2101239 (2021). https://doi.org/10.1002/adfm.202101239

64. J. Béjar, F. Espinosa-Magaña, M. Guerra-Balcázar, J. Ledesma-García, L. Álvarez-Contreras et al., Three-dimensional-order macroporous AB_2O_4 spinels (A, B = Co and Mn) as electrodes in Zn–air batteries. ACS Appl. Mater. Interfaces **12**, 53760–53773 (2020). https://doi.org/10.1021/acsami.0c14920

65. J. Wang, Y. Liu, N. Li, F. Qin, F. Xu et al., Petal-like N, O-codoped carbon nanosheets as Mott-Schottky nanoreactors in electrodes of Zn–air batteries and supercapacitors. Carbon **178**, 581–593 (2021). https://doi.org/10.1016/j.carbon.2021.03.015

66. Y. Du, S. Guo, Chemically doped fluorescent carbon and graphene quantum dots for bioimaging, sensor, catalytic and photoelectronic applications. Nanoscale **8**, 2532–2543 (2016). https://doi.org/10.1039/c5nr07579c

67. X. Li, M. Rui, J. Song, Z. Shen, H. Zeng, Carbon and graphene quantum dots for optoelectronic and energy devices: a review. Adv. Funct. Mater. **25**, 4929–4947 (2015). https://doi.org/10.1002/adfm.201501250

68. T. Fan, G. Zhang, L. Jian, I. Murtaza, H. Meng et al., Facile synthesis of defect-rich nitrogen and sulfur Co-doped graphene quantum dots as metal-free electrocatalyst for the oxygen reduction reaction. J. Alloys Compd. **792**, 844–850 (2019). https://doi.org/10.1016/j.jallcom.2019.04.097

69. W. Zheng, J. Lv, H. Zhang, H.-X. Zhang, J. Zhang, Co_9S_8 integrated into nitrogen/sulfur dual-doped carbon nanofibers as an efficient oxygen bifunctional electrocatalyst for Zn–air batteries. Sustain. Energy Fuels **4**, 1093–1098 (2020). https://doi.org/10.1039/C9SE01130G

70. W. Xie, J. Li, Y. Song, S. Li, J. Li et al., Hierarchical carbon microtube@nanotube core-shell structure for high-performance oxygen electrocatalysis and Zn–air battery. Nano-Micro Lett. **12**, 97 (2020). https://doi.org/10.1007/s40820-020-00435-z

71. R. Tang, Y. Li, J. Liu, W. Zhou, H. Wu et al., Cobalt nanoparticles embedded nitrogen-doped carbon nanotubes as bifunctional catalysts for flexible solid-state Zn–air battery. J. Electrochem. Soc. **167**, 060521 (2020). https://doi.org/10.1149/1945-7111/ab84f6

72. Q. Wei, F. Xiong, S. Tan, L. Huang, E.H. Lan et al., Porous one-dimensional nanomaterials: design, fabrication and applications in electrochemical energy storage. Adv. Mater. **29**, 1602300 (2017). https://doi.org/10.1002/adma.201602300

73. X. Li, Y. Liu, H. Chen, M. Yang, D. Yang et al., Rechargeable Zn-air batteries with outstanding cycling stability enabled by ultrafine FeNi nanoparticles-encapsulated N-doped carbon nanosheets as a bifunctional electrocatalyst. Nano Lett. **21**, 3098–3105 (2021). https://doi.org/10.1021/acs.nanolett.1c00279

74. F. Li, T. Qin, Y. Sun, R. Jiang, J. Yuan et al., Preparation of a one-dimensional hierarchical MnO@CNT@Co–N/C ternary nanostructure as a high-performance bifunctional electrocatalyst for rechargeable Zn–air batteries. J. Mater. Chem. A **9**, 22533–22543 (2021). https://doi.org/10.1039/D1TA07259E

75. C. Li, J. Cheng, Y. Jiang, W. Xiao, X. Yan, Electronic structure regulation and electrocatalytic mechanism of one-dimensional mesoporous $La_{0.8}Sr_{0.2}Mn_{1-x}Co_xO_3$ with bifunctional electrocatalysts towards Zn–air batteries. J. Power. Sources **498**, 229940 (2021). https://doi.org/10.1016/j.jpowsour.2021.229940

76. X. Shu, S. Chen, S. Chen, W. Pan, J. Zhang, Cobalt nitride embedded holey N-doped graphene as advanced bifunctional electrocatalysts for Zn–air batteries and overall water splitting. Carbon **157**, 234–243 (2020). https://doi.org/10.1016/j.carbon.2019.10.023

77. Z. Li, H. Li, M. Li, J. Hu, Y. Liu et al., Iminodiacetonitrile induce-synthesis of two-dimensional PdNi/Ni@carbon nanosheets with uniform dispersion and strong interface

bonding as an effective bifunctional eletrocatalyst in air-cathode. Energy Storage Mater. **42**, 118–128 (2021). https://doi.org/10.1016/j.ensm.2021.07.027

78. L. Zhao, B. Dong, S. Li, L. Zhou, L. Lai et al., Interdiffusion reaction-assisted hybridization of two-dimensional metal-organic frameworks and $Ti_3C_2T_x$ nanosheets for electrocatalytic oxygen evolution. ACS Nano **11**, 5800–5807 (2017). https://doi.org/10.1021/acsnano.7b01409

79. A. Murali, G. Lokhande, K.A. Deo, A. Brokesh, A.K. Gaharwar, Emerging 2D nanomaterials for biomedical applications. Mater. Today **50**, 276–302 (2021). https://doi.org/10.1016/j.mattod.2021.04.020

80. W.-J. Niu, J.-Z. He, Y.-P. Wang, Q.-Q. Sun, W.-W. Liu et al., A hybrid transition metal nanocrystal-embedded graphitic carbon nitride nanosheet system as a superior oxygen electrocatalyst for rechargeable Zn–air batteries. Nanoscale **12**, 19644–19654 (2020). https://doi.org/10.1039/d0nr03987j

81. J.-T. Ren, Y.-S. Wang, L. Chen, L.-J. Gao, W.-W. Tian et al., Binary FeNi phosphides dispersed on N, P-doped carbon nanosheets for highly efficient overall water splitting and rechargeable Zn–air batteries. Chem. Eng. J. **389**, 124408 (2020). https://doi.org/10.1016/j.cej.2020.124408

82. L. Xu, Y. Tian, D. Deng, H. Li, D. Zhang et al., Cu nanoclusters/FeN_4 amorphous composites with dual active sites in N-doped graphene for high-performance Zn–air batteries. ACS Appl. Mater. Interfaces **12**, 31340–31350 (2020). https://doi.org/10.1021/acsami.0c03823

83. X. Wang, Y. Liu, Z. Wei, J. Hong, H. Liang et al., MXene-boosted imine cathodes with extended conjugated structure for aqueous zinc-ion batteries. Adv. Mater. **34**, e2206812 (2022). https://doi.org/10.1002/adma.202206812

84. R. Zhu, H. Duan, Z. Zhao, H. Pang, Recent progress of dimensionally designed electrode nanomaterials in aqueous electrochemical energy storage. J. Mater. Chem. A **9**, 9535–9572 (2021). https://doi.org/10.1039/D1TA00204J

85. C. Zhang, F. Kong, Y. Qiao, Q. Zhao, A. Kong et al., 3D graphene-carbon nanotube hybrid supported coupled Co-MnO nanoparticles as highly efficient bifunctional electrocatalyst for rechargeable Zn–air batteries. Chem. Asian J. **15**, 3535–3541 (2020). https://doi.org/10.1002/asia.202000913

86. C. Xia, L. Huang, D. Yan, A.I. Douka, W. Guo et al., Electrospinning synthesis of self-standing cobalt/nanocarbon hybrid membrane for long-life rechargeable zinc–air batteries. Adv. Funct. Mater. **31**, 2105021 (2021). https://doi.org/10.1002/adfm.202105021

87. G. Liu, J. Li, J. Fu, G. Jiang, G. Lui et al., An oxygen-vacancy-rich semiconductor-supported bifunctional catalyst for efficient and stable zinc–air batteries. Adv. Mater. **31**, e1806761 (2019). https://doi.org/10.1002/adma.201806761

88. D. Wang, Y.-P. Deng, Y. Zhang, Y. Zhao, G. Zhou et al., Defect engineering on three-dimensionally ordered macroporous phosphorus doped $Co_3O_{4-\delta}$ microspheres as an efficient bifunctional electrocatalyst for Zn–air batteries. Energy Storage Mater. **41**, 427–435 (2021). https://doi.org/10.1016/j.ensm.2021.06.017

89. Y.-P. Deng, Y. Jiang, D. Luo, J. Fu, R. Liang et al., Hierarchical porous double-shelled electrocatalyst with tailored lattice alkalinity toward bifunctional oxygen reactions for metal–air batteries. ACS Energy Lett. **2**, 2706–2712 (2017). https://doi.org/10.1021/acsenergylett.7b00989

90. Y. Xue, Y. Guo, Q. Zhang, Z. Xie, J. Wei et al., MOF-derived Co and Fe species loaded on N-doped carbon networks as efficient oxygen electrocatalysts for Zn–air batteries. Nano-Micro Lett. **14**, 162 (2022). https://doi.org/10.1007/s40820-022-00890-w

91. L. Wang, M. Xu, H. Li, Z. Huang, L. Wang et al., Mn-doped Zn metal-organic framework-derived porous N-doped carbon composite as a high-performance nonprecious electrocatalyst for oxygen reduction and aqueous/flexible zinc-air batteries. Inorg. Chem. **62**, 13284–13292 (2023). https://doi.org/10.1021/acs.inorgchem.3c01536

92. R. Hao, J. Chen, Z. Wang, Y. Huang, P. Liu et al., Trimetallic Zeolitic imidazolite framework-derived Co nanoparticles@CoFe-nitrogen-doped porous carbon as bifunctional electrocatalysts for Zn–air battery. J. Colloid Interface Sci. **586**, 621–629 (2021). https://doi.org/10.1016/j.jcis.2020.10.130

93. Y. Chen, C. Gong, Z. Shi, D. Chen, X. Chen et al., Molten-salt-assisted synthesis of onion-like Co/CoO@FeNC materials with boosting reversible oxygen electrocatalysis for rechargeable Zn–air battery. J. Colloid Interface Sci. **596**, 206–214 (2021). https://doi.org/10.1016/j.jcis.2021.03.145

94. Y. Xu, P. Deng, G. Chen, J. Chen, Y. Yan et al., 2D nitrogen-doped carbon nanotubes/graphene hybrid as bifunctional oxygen electrocatalyst for long-life rechargeable Zn–air batteries. Adv. Funct. Mater. **30**, 1906081 (2020). https://doi.org/10.1002/adfm.201906081

95. Z. Zeng, G. Fu, H.B. Yang, Y. Yan, J. Chen et al., Bifunctional N-$CoSe_2$/3D-MXene as highly efficient and durable cathode for rechargeable Zn–air battery. ACS Mater. Lett. **1**, 432–439 (2019). https://doi.org/10.1021/acsmaterialslett.9b00337

96. T. Fu, G. Li, Y. Xiang, Y. Tang, D. Cai et al., Hierarchical cobalt-nitrogen-doped carbon composite as efficiently bifunctional oxygen electrocatalyst for rechargeable Zn–air batteries. J. Alloys Compd. **878**, 160349 (2021). https://doi.org/10.1016/j.jallcom.2021.160349

97. Y. Zheng, S. Chen, K.A.I. Zhang, J. Zhu, J. Xu et al., Ultrasound-triggered assembly of covalent triazine framework for synthesizing heteroatom-doped carbon nanoflowers boosting metal-free bifunctional electrocatalysis. ACS Appl. Mater. Interfaces **13**, 13328–13337 (2021). https://doi.org/10.1021/acsami.1c01348

98. X. Guo, X. Zheng, X. Hu, Q. Zhao, L. Li et al., Electrostatic adsorbing graphene quantum dot into nickel–based layered double hydroxides: electron absorption/donor effects enhanced oxygen electrocatalytic activity. Nano Energy **84**, 105932 (2021). https://doi.org/10.1016/j.nanoen.2021.105932

99. F. Xu, J. Wang, Y. Zhang, W. Wang, T. Guan et al., Structure-engineered bifunctional oxygen electrocatalysts with

Ni₃S₂ quantum dot embedded S/N-doped carbon nanosheets for rechargeable Zn-air batteries. Chem. Eng. J. **432**, 134256 (2022). https://doi.org/10.1016/j.cej.2021.134256

100. X. Wang, R.K.M. Raghupathy, C.J. Querebillo, Z. Liao, D. Li et al., Interfacial covalent bonds regulated electron-deficient 2D black phosphorus for electrocatalytic oxygen reactions. Adv. Mater. **33**, e2008752 (2021). https://doi.org/10.1002/adma.202008752

101. J.-C. Li, Y. Meng, L. Zhang, G. Li, Z. Shi et al., Dual-phasic carbon with Co single atoms and nanoparticles as a bifunctional oxygen electrocatalyst for rechargeable Zn–air batteries. Adv. Funct. Mater. **31**, 2103360 (2021). https://doi.org/10.1002/adfm.202103360

102. S. Wang, J. Wang, X. Wang, L. Li, J. Qin et al., Carbon hybrid with 3D nano-forest architecture in-situ catalytically constructed by CoFe alloy as advanced multifunctional electrocatalysts for Zn–air batteries-driven water splitting. J. Energy Chem. **53**, 422–432 (2021). https://doi.org/10.1016/j.jechem.2020.07.045

103. C.-C. Weng, J.-T. Ren, H.-Y. Wang, X.-W. Lv, Y.-J. Song et al., Triple-phase oxygen electrocatalysis of hollow spherical structures for rechargeable Zn–air batteries. Appl. Catal. B Environ. **307**, 121190 (2022). https://doi.org/10.1016/j.apcatb.2022.121190

104. Z. Liang, N. Kong, C. Yang, W. Zhang, H. Zheng et al., Highly curved nanostructure-coated Co, N-doped carbon materials for oxygen electrocatalysis. Angew. Chem. Int. Ed. **60**, 12759–12764 (2021). https://doi.org/10.1002/anie.202101562

105. L. Yan, Z. Xu, W. Hu, J. Ning, Y. Zhong et al., Formation of sandwiched leaf-like CNTs-Co/ZnCo₂O₄@NC-CNTs nanohybrids for high-power-density rechargeable Zn-air batteries. Nano Energy **82**, 105710 (2021). https://doi.org/10.1016/j.nanoen.2020.105710

106. B. Wang, Y. Ye, L. Xu, Y. Quan, W. Wei et al., Space-confined yolk-shell construction of Fe₃O₄ nanoparticles inside N-doped hollow mesoporous carbon spheres as bifunctional electrocatalysts for long-term rechargeable zinc–air batteries. Adv. Funct. Mater. **30**, 2005834 (2020). https://doi.org/10.1002/adfm.202005834

107. J. Sun, H. Xue, N. Guo, T. Song, Y.-R. Hao et al., Synergetic metal defect and surface chemical reconstruction into NiCo₂S₄/ZnS heterojunction to achieve outstanding oxygen evolution performance. Angew. Chem. Int. Ed. **60**, 19435–19441 (2021). https://doi.org/10.1002/anie.202107731

108. Y. Wei, Z. Weng, L. Guo, L. An, J. Yin et al., Activation strategies of perovskite-type structure for applications in oxygen-related electrocatalysts. Small Methods **5**, e2100012 (2021). https://doi.org/10.1002/smtd.202100012

109. Y. Feng, Z. Zhao, F. Li, L. Bu, Q. Shao et al., Highly surface-distorted Pt superstructures for multifunctional electrocatalysis. Nano Lett. **21**, 5075–5082 (2021). https://doi.org/10.1021/acs.nanolett.1c00902

110. R. Majee, T. Das, S. Chakraborty, S. Bhattacharyya, Shaping a doped perovskite oxide with measured grain boundary defects to catalyze bifunctional oxygen activation for a rechargeable Zn–air battery. ACS Appl. Mater. Interfaces **12**, 40355–40363 (2020). https://doi.org/10.1021/acsami.0c11606

111. C. Li, X. Han, F. Cheng, Y. Hu, C. Chen et al., Phase and composition controllable synthesis of cobalt manganese spinel nanoparticles towards efficient oxygen electrocatalysis. Nat. Commun. **6**, 7345 (2015). https://doi.org/10.1038/ncomms8345

112. D.U. Lee, J. Li, M.G. Park, M.H. Seo, W. Ahn et al., Self-assembly of spinel nanocrystals into mesoporous spheres as bifunctionally active oxygen reduction and evolution electrocatalysts. ChemSusChem **10**, 2258–2266 (2017). https://doi.org/10.1002/cssc.201700369

113. X. Zhao, J. Chen, Z. Bi, S. Chen, L. Feng et al., Electron modulation and morphology engineering jointly accelerate oxygen reaction to enhance Zn-air battery performance. Adv. Sci. **10**, e2205889 (2023). https://doi.org/10.1002/advs.202205889

114. M. Zhao, Y. Xia, Crystal-phase and surface-structure engineering of ruthenium nanocrystals. Nat. Rev. Mater. **5**, 440–459 (2020). https://doi.org/10.1038/s41578-020-0183-3

115. G. Wu, J. Wang, W. Ding, Y. Nie, L. Li et al., A strategy to promote the electrocatalytic activity of spinels for oxygen reduction by structure reversal. Angew. Chem. Int. Ed. **55**, 1340–1344 (2016). https://doi.org/10.1002/anie.201508809

116. X. Han, G. He, Y. He, J. Zhang, X. Zheng et al., Engineering catalytic active sites on cobalt oxide surface for enhanced oxygen electrocatalysis. Adv. Energy Mater. **8**, 1702222 (2018). https://doi.org/10.1002/aenm.201702222

117. Q. Xie, Z. Wang, C. Lei, P. Guo, C. Li et al., Fe-Doping induced divergent growth of Ni–Fe alloy nanoparticles for enhancing the electrocatalytic oxygen reduction. Catal. Sci. Technol. **11**, 5171–5179 (2021). https://doi.org/10.1039/D1CY00668A

118. Y. Wang, R. Gan, Z. Ai, H. Liu, C. Wei et al., Hollow Co₃O₄₋ₓ nanoparticles decorated N-doped porous carbon prepared by one-step pyrolysis as an efficient ORR electrocatalyst for rechargeable Zn–air batteries. Carbon **181**, 87–98 (2021). https://doi.org/10.1016/j.carbon.2021.05.016

119. K. Chu, F. Liu, J. Zhu, H. Fu, H. Zhu et al., A general strategy to boost electrocatalytic nitrogen reduction on perovskite oxides via the oxygen vacancies derived from a-site deficiency. Adv. Energy Mater. **11**, 2003799 (2021). https://doi.org/10.1002/aenm.202003799

120. H. Han, S. Jin, S. Park, Y. Kim, D. Jang et al., Plasma-induced oxygen vacancies in amorphous MnOₓ boost catalytic performance for electrochemical CO₂ reduction. Nano Energy **79**, 105492 (2021). https://doi.org/10.1016/j.nanoen.2020.105492

121. X.-T. Wang, T. Ouyang, L. Wang, J.-H. Zhong, Z.-Q. Liu, Surface reorganization on electrochemically-induced Zn–Ni–Co spinel oxides for enhanced oxygen electrocatalysis. Angew. Chem. Int. Ed. **59**, 6492–6499 (2020). https://doi.org/10.1002/anie.202000690

122. X. Li, H. Zhang, Y. Wang, H. Wang, J. Wang et al., Tailoring the spin state of active sites in amorphous transition metal sulfides to promote oxygen electrocatalysis. Sci. China Mater. **65**, 3479–3489 (2022). https://doi.org/10.1007/s40843-022-2048-2

123. X. Liu, Q. Yin, C. Dai, G. Li, J. Lian et al., Amorphous bimetallic phosphate–carbon precatalyst with deep self-reconstruction toward efficient oxygen evolution reaction and Zn–air batteries. ACS Sustain. Chem. Eng. **9**, 5345–5355 (2021). https://doi.org/10.1021/acssuschemeng.0c09339

124. Y.-X. Duan, F.-L. Meng, K.-H. Liu, S.-S. Yi, S.-J. Li et al., Amorphizing of Cu nanoparticles toward highly efficient and robust electrocatalyst for CO_2 reduction to liquid fuels with high faradaic efficiencies. Adv. Mater. **30**, e1706194 (2018). https://doi.org/10.1002/adma.201706194

125. M. Wu, G. Zhang, H. Tong, X. Liu, L. Du et al., Cobalt (II) oxide nanosheets with rich oxygen vacancies as highly efficient bifunctional catalysts for ultra-stable rechargeable Zn–air flow battery. Nano Energy **79**, 105409 (2021). https://doi.org/10.1016/j.nanoen.2020.105409

126. J. Choi, T.-G. Jeong, B.W. Cho, Y. Jung, S.H. Oh et al., Tungsten carbide as a highly efficient catalyst for polysulfide fragmentations in Li–S batteries. J. Phys. Chem. C **122**, 7664–7669 (2018). https://doi.org/10.1021/acs.jpcc.8b02096

127. M.R. Lukatskaya, O. Mashtalir, C.E. Ren, Y. Dall'Agnese, P. Rozier et al., Cation intercalation and high volumetric capacitance of two-dimensional titanium carbide. Science **341**, 1502–1505 (2013). https://doi.org/10.1126/science.1241488

128. B. Wang, G. Wang, H. Wang, Hybrids of Mo_2C nanoparticles anchored on graphene sheets as anode materials for high performance lithium-ion batteries. J. Mater. Chem. A **3**, 17403–17411 (2015). https://doi.org/10.1039/c5ta03929k

129. S. Song, W. Xu, R. Cao, L. Luo, M.H. Engelhard et al., B_4C as a stable non-carbon-based oxygen electrode material for lithium-oxygen batteries. Nano Energy **33**, 195–204 (2017). https://doi.org/10.1016/j.nanoen.2017.01.042

130. D.K. Bediako, B. Lassalle-Kaiser, Y. Surendranath, J. Yano, V.K. Yachandra et al., Structure-activity correlations in a nickel-borate oxygen evolution catalyst. J. Am. Chem. Soc. **134**, 6801–6809 (2012). https://doi.org/10.1021/ja301018q

131. J.M.V. Nsanzimana, Y. Peng, Y.Y. Xu, L. Thia, C. Wang et al., An efficient and earth-abundant oxygen-evolving electrocatalyst based on amorphous metal borides. Adv. Energy Mater. **8**, 1701475 (2018). https://doi.org/10.1002/aenm.201701475

132. W. Zhao, T. Xu, T. Li, Y. Wang, H. Liu et al., Amorphous iron(III)-borate nanolattices as multifunctional electrodes for self-driven overall water splitting and rechargeable zinc-air battery. Small **14**, e1802829 (2018). https://doi.org/10.1002/smll.201802829

133. A. Saad, Y. Gao, A. Ramiere, T. Chu, G. Yasin et al., Understanding the surface reconstruction on ternary W_xCoB_x for water oxidation and zinc-air battery applications. Small **18**, e2201067 (2022). https://doi.org/10.1002/smll.202201067

134. T. Liu, Q. Liu, A.M. Asiri, Y. Luo, X. Sun, An amorphous CoSe film behaves as an active and stable full water-splitting electrocatalyst under strongly alkaline conditions. Chem. Commun. **51**, 16683–16686 (2015). https://doi.org/10.1039/C5CC06892D

135. H. Zou, G. Li, L. Duan, Z. Kou, J. Wang, In situ coupled amorphous cobalt nitride with nitrogen-doped graphene aerogel as a trifunctional electrocatalyst towards Zn–air battery deriven full water splitting. Appl. Catal. B Environ. **259**, 118100 (2019). https://doi.org/10.1016/j.apcatb.2019.118100

136. X. Zheng, Y. Qian, H. Gong, W. Shi, J. Yan et al., Bridge-linking interfacial engineering of triple carbons for highly efficient and binder-free electrodes toward flexible Zn–air batteries. Appl. Catal. B Environ. **319**, 121937 (2022). https://doi.org/10.1016/j.apcatb.2022.121937

137. K. Ding, Y. Ye, J. Hu, L. Zhao, W. Jin et al., Aerophilic triphase interface tuned by carbon dots driving durable and flexible rechargeable Zn–air batteries. Nano-Micro Lett. **15**, 28 (2023). https://doi.org/10.1007/s40820-022-00994-3

138. Y. Niu, X. Teng, S. Gong, M. Xu, S.-G. Sun et al., Engineering two-phase bifunctional oxygen electrocatalysts with tunable and synergetic components for flexible Zn–air batteries. Nano-Micro Lett. **13**, 126 (2021). https://doi.org/10.1007/s40820-021-00650-2

139. Y. Jiang, Y.-P. Deng, J. Fu, D.U. Lee, R. Liang et al., Zn–air Batteries: interpenetrating triphase cobalt-based nanocomposites as efficient bifunctional oxygen electrocatalysts for long-lasting rechargeable Zn–air batteries. Adv. Energy Mater. **8**, 1870068 (2018). https://doi.org/10.1002/aenm.201870068

140. Y. Go, K. Min, H. An, K. Kim, S.E. Shim et al., Oxygen-vacancy-rich $CoFe/CoFe_2O_4$ embedded in N-doped hollow carbon spheres as a highly efficient bifunctional electrocatalyst for Zn–air batteries. Chem. Eng. J. **448**, 137665 (2022). https://doi.org/10.1016/j.cej.2022.137665

141. X. Wu, Z. Zhang, C. He, Y. Shen, X. Wu et al., Mixed-valence cobalt oxides bifunctional electrocatalyst with rich oxygen vacancies for aqueous metal-air batteries. Chem. Eng. J. **453**, 139831 (2023). https://doi.org/10.1016/j.cej.2022.139831

142. Y. Niu, M. Xiao, J. Zhu, T. Zeng, J. Li et al., A "trimurti" heterostructured hybrid with an intimate CoO/Co_xP interface as a robust bifunctional air electrode for rechargeable Zn–air batteries. J. Mater. Chem. A **8**, 9177–9184 (2020). https://doi.org/10.1039/D0TA01145B

143. M. Guo, Z. Huang, Y. Qu, L. Wang, H. Li et al., Synergistic effect and nanostructure engineering of three-dimensionally hollow mesoporous spherical Cu_3P/TiO_2 in aqueous/flexible Zn–air batteries. Appl. Catal. B Environ. **320**, 121991 (2023). https://doi.org/10.1016/j.apcatb.2022.121991

144. Q. Lu, X. Zou, C. Wang, K. Liao, P. Tan et al., Tailoring charge and mass transport in cation/anion-Co doped Ni_3N/N-doped CNT integrated electrode toward rapid oxygen evolution for fast-charging zinc–air batteries. Energy Storage Mater. **39**, 11–20 (2021). https://doi.org/10.1016/j.ensm.2021.04.013

145. W. Li, F. Wang, Z. Zhang, S. Min, Graphitic carbon layer-encapsulated Co nanoparticles embedded on porous

carbonized wood as a self-supported chainmail oxygen electrode for rechargeable Zn–air batteries. Appl. Catal. B Environ. **317**, 121758 (2022). https://doi.org/10.1016/j.apcatb.2022.121758

146. L. Yan, B. Xie, C. Yang, Y. Wang, J. Ning et al., Engineering self-supported hydrophobic–aerophilic air cathode with CoS/Fe$_3$S$_4$ nanoparticles embedded in S, N Co-doped carbon plate arrays for long-life rechargeable Zn–air batteries. Adv. Energy Mater. **13**, 2370040 (2023). https://doi.org/10.1002/aenm.202370040

147. X. Shi, B. He, L. Zhao, Y. Gong, R. Wang et al., FeS$_2$–CoS$_2$ incorporated into nitrogen-doped carbon nanofibers to boost oxygen electrocatalysis for durable rechargeable Zn–air batteries. J. Power. Sources **482**, 228955 (2021). https://doi.org/10.1016/j.jpowsour.2020.228955

148. W. Jin, J. Chen, B. Liu, J. Hu, Z. Wu et al., Oxygen vacancy-rich In-doped CoO/CoP heterostructure as an effective air cathode for rechargeable Zn–air batteries. Small **15**, e1904210 (2019). https://doi.org/10.1002/smll.201904210

149. W. Zhang, C.-H. Xu, H. Zheng, R. Li, K. Zhou, Oxygen-rich cobalt–nitrogen–carbon porous nanosheets for bifunctional oxygen electrocatalysis. Adv. Funct. Mater. **32**, 2200763 (2022). https://doi.org/10.1002/adfm.202200763

150. Y. Sun, S. Gao, F. Lei, J. Liu, L. Liang et al., Atomically-thin non-layered cobalt oxide porous sheets for highly efficient oxygen-evolving electrocatalysts. Chem. Sci. **5**, 3976–3982 (2014). https://doi.org/10.1039/C4SC00565A

151. J. Yin, J. Jin, H. Liu, B. Huang, M. Lu et al., NiCo$_2$O$_4$-based nanosheets with uniform 4 nm mesopores for excellent Zn–air battery performance. Adv. Mater. **32**, e2001651 (2020). https://doi.org/10.1002/adma.202001651

152. J. Qin, Z. Liu, D. Wu, J. Yang, Optimizing the electronic structure of cobalt via synergized oxygen vacancy and Co–N–C to boost reversible oxygen electrocatalysis for rechargeable Zn–air batteries. Appl. Catal. B Environ. **278**, 119300 (2020). https://doi.org/10.1016/j.apcatb.2020.119300

153. K. Kim, K. Min, Y. Go, Y. Lee, S.E. Shim et al., FeCo alloy nanoparticles embedded in N-doped carbon supported on highly defective ketjenblack as effective bifunctional electrocatalysts for rechargeable Zn–air batteries. Appl. Catal. B Environ. **315**, 121501 (2022). https://doi.org/10.1016/j.apcatb.2022.121501

154. C. Lai, H. Li, Y. Sheng, M. Zhou, W. Wang et al., 3D spatial combination of CN vacancy-mediated NiFe-PBA with N-doped carbon nanofibers network toward free-standing bifunctional electrode for Zn–air batteries. Adv. Sci. **9**, e2105925 (2022). https://doi.org/10.1002/advs.202105925

155. Q. He, Y. Wan, H. Jiang, Z. Pan, C. Wu et al., Nickel vacancies boost reconstruction in nickel hydroxide electrocatalyst. ACS Energy Lett. **3**, 1373–1380 (2018). https://doi.org/10.1021/acsenergylett.8b00515

156. J.-J. Wang, X.-P. Li, B.-F. Cui, Z. Zhang, X.-F. Hu et al., A review of non-noble metal-based electrocatalysts for CO$_2$ electroreduction. Rare Met. **40**, 3019–3037 (2021). https://doi.org/10.1007/s12598-021-01736-x

157. L. Tao, Q. Wang, S. Dou, Z. Ma, J. Huo et al., Edge-rich and dopant-free graphene as a highly efficient metal-free electrocatalyst for the oxygen reduction reaction. Chem. Commun. **52**, 2764–2767 (2016). https://doi.org/10.1039/c5cc09173j

158. J. Fu, F.M. Hassan, C. Zhong, J. Lu, H. Liu et al., Defect engineering of chalcogen-tailored oxygen electrocatalysts for rechargeable quasi-solid-state zinc-air batteries. Adv. Mater. **29**, 1702526 (2017). https://doi.org/10.1002/adma.201702526

159. F. Yang, J.H. Xie, D.W. Rao, X.Q. Liu et al., Octahedral distortion enhances exceptional oxygen catalytic activity of calcium manganite for advanced Zn–Air batteries. Nano Energy **85**, 106020 (2021). https://doi.org/10.1016/j.nanoen.2021.106020

160. F. Yang, J. Xie, X. Liu, G. Wang, X. Lu, Linker defects triggering boosted oxygen reduction activity of Co/Zn–ZIF nanosheet arrays for rechargeable Zn–air batteries. Small **17**, e2007085 (2021). https://doi.org/10.1002/smll.202007085

161. H. Pan, X. Huang, Z. Lu, Z. Zhang, B. An et al., Dual oxidation and sulfurization enabling hybrid Co/Co$_3$O$_4$@CoS in S/N-doped carbon matrix for bifunctional oxygen electrocatalysis and rechargeable Zn–air batteries. Chem. Eng. J. **419**, 129619 (2021). https://doi.org/10.1016/j.cej.2021.129619

162. C. Lai, M. Gong, Y. Zhou, J. Fang, L. Huang et al., Sulphur modulated Ni$_3$FeN supported on N/S Co-doped graphene boosts rechargeable/flexible Zn–air battery performance. Appl. Catal. B Environ. **274**, 119086 (2020). https://doi.org/10.1016/j.apcatb.2020.119086

163. Q. Wang, Y. Ji, Y. Lei, Y. Wang, Y. Wang et al., Pyridinic-N-dominated doped defective graphene as a superior oxygen electrocatalyst for ultrahigh-energy-density Zn–air batteries. ACS Energy Lett. **3**, 1183–1191 (2018). https://doi.org/10.1021/acsenergylett.8b00303

164. J. Li, Y. Kang, D. Liu, Z. Lei, P. Liu, Nitrogen-doped graphitic carbon-supported ultrafine co nanoparticles as an efficient multifunctional electrocatalyst for HER and rechargeable Zn–air batteries. ACS Appl. Mater. Interfaces **12**, 5717–5729 (2020). https://doi.org/10.1021/acsami.9b18101

165. W. Lei, Y.-P. Deng, G. Li, Z.P. Cano, X. Wang et al., Two-dimensional phosphorus-doped carbon nanosheets with tunable porosity for oxygen reactions in zinc–air batteries. ACS Catal. **8**, 2464–2472 (2018). https://doi.org/10.1021/acscatal.7b02739

166. P. Thangasamy, S. Oh, H. Randriamahazaka, S. Nam, I.-K. Oh, Mechanistic insight into collectively exhaustive CoPi–NPC nanosheets for oxygen reduction reaction and Zn–air battery. Appl. Catal. B Environ. **316**, 121656 (2022). https://doi.org/10.1016/j.apcatb.2022.121656

167. T.V. Vineesh, M.P. Kumar, C. Takahashi, G. Kalita, S. Alwarappan et al., Bifunctional electrocatalytic activity of boron-doped graphene derived from boron carbide. Adv. Energy Mater. **5**, 1500658 (2015). https://doi.org/10.1002/aenm.201500658

168. Y. Kang, W. Wang, J. Li, S. Imhanria, Y. Hao et al., Ultrathin B, N Co-doped porous carbon nanosheets derived from intumescent flame retardant for rechargeable Zn–air

battery. J. Power. Sources **493**, 229665 (2021). https://doi.org/10.1016/j.jpowsour.2021.229665

169. X. Zheng, J. Wu, X. Cao, J. Abbott, C. Jin et al., N-, P-, and S-doped graphene-like carbon catalysts derived from onium salts with enhanced oxygen chemisorption for Zn–air battery cathodes. Appl. Catal. B Environ. **241**, 442–451 (2019). https://doi.org/10.1016/j.apcatb.2018.09.054

170. J. Ran, T. Wang, J. Zhang, Y. Liu, C. Xu et al., Modulation of electronics of oxide perovskites by sulfur doping for electrocatalysis in rechargeable Zn–air batteries. Chem. Mater. **32**, 3439–3446 (2020). https://doi.org/10.1021/acs.chemmater.9b05148

171. D. Zhang, P. Sun, Q. Zhou, B. Li, Y. Wei et al., Enhanced oxygen reduction and evolution in N-doped carbon anchored with Co nanoparticles for rechargeable Zn–air batteries. Appl. Surf. Sci. **542**, 148700 (2021). https://doi.org/10.1016/j.apsusc.2020.148700

172. H. Yang, S. Gao, D. Rao, X. Yan, Designing superior bifunctional electrocatalyst with high-purity pyrrole-type CoN_4 and adjacent metallic cobalt sites for rechargeable Zn–air batteries. Energy Storage Mater. **46**, 553–562 (2022). https://doi.org/10.1016/j.ensm.2022.01.040

173. Q. Lv, N. Wang, W. Si, Z. Hou, X. Li et al., Pyridinic nitrogen exclusively doped carbon materials as efficient oxygen reduction electrocatalysts for Zn–air batteries. Appl. Catal. B Environ. **261**, 118234 (2020). https://doi.org/10.1016/j.apcatb.2019.118234

174. T. Lu, X. Hu, J. He, R. Li, J. Gao et al., Aqueous/solid state Zn–air batteries based on N doped graphdiyne as efficient metal-free bifunctional catalyst. Nano Energy **85**, 106024 (2021). https://doi.org/10.1016/j.nanoen.2021.106024

175. Y.-N. Sun, J. Yang, X. Ding, W. Ji, A. Jaworski et al., Synergetic contribution of nitrogen and fluorine species in porous carbons as metal-free and bifunctional oxygen electrocatalysts for zinc–air batteries. Appl. Catal. B Environ. **297**, 120448 (2021). https://doi.org/10.1016/j.apcatb.2021.120448

176. K. Tang, C. Yuan, Y. Xiong, H. Hu, M. Wu, Inverse-opal-structured hybrids of N, S-codoped-carbon-confined Co_9S_8 nanoparticles as bifunctional oxygen electrocatalyst for on-chip all-solid-state rechargeable Zn–air batteries. Appl. Catal. B Environ. **260**, 118209 (2020). https://doi.org/10.1016/j.apcatb.2019.118209

177. P. Li, H. Wang, W. Fan, M. Huang, J. Shi et al., Salt assisted fabrication of lignin-derived Fe, N, P, S codoped porous carbon as trifunctional catalyst for Zn-air batteries and water-splitting devices. Chem. Eng. J. **421**, 129704 (2021). https://doi.org/10.1016/j.cej.2021.129704

178. Y. Meng, J.-C. Li, S.-Y. Zhao, C. Shi, X.-Q. Li et al., Fluorination-assisted preparation of self-supporting single-atom Fe–N-doped single-wall carbon nanotube film as bifunctional oxygen electrode for rechargeable Zn–air batteries. Appl. Catal. B Environ. **294**, 120239 (2021). https://doi.org/10.1016/j.apcatb.2021.120239

179. Y. Zhou, R. Lu, X. Tao, Z. Qiu, G. Chen et al., Boosting oxygen electrocatalytic activity of Fe–N–C catalysts by phosphorus incorporation. J. Am. Chem. Soc. **145**, 3647–3655 (2023). https://doi.org/10.1021/jacs.2c12933

180. H.-F. Wang, C. Tang, B. Wang, B.-Q. Li, X. Cui et al., Defect-rich carbon fiber electrocatalysts with porous graphene skin for flexible solid-state zinc–air batteries. Energy Storage Mater. **15**, 124–130 (2018). https://doi.org/10.1016/j.ensm.2018.03.022

181. Z. Niu, Z. Lu, Z. Qiao, M. Xing, L. Han et al., Long-range regulation of Se doping for oxygen reduction of atomically dispersed Sb catalysts for ultralow-temperature solid-state Zn–air batteries. ACS Catal. **13**, 7122–7131 (2023). https://doi.org/10.1021/acscatal.3c01125

182. Y. Huang, Y. Wang, C. Tang, J. Wang, Q. Zhang et al., Atomic modulation and structure design of carbons for bifunctional electrocatalysis in metal-air batteries. Adv. Mater. **31**, e1803800 (2019). https://doi.org/10.1002/adma.201803800

183. C. Tang, Q. Zhang, Nanocarbon for oxygen reduction electrocatalysis: dopants, edges, and defects. Adv. Mater. **29**, 1604103 (2017). https://doi.org/10.1002/adma.201604103

184. Z. Liu, Z. Zhao, Y. Wang, S. Dou, D. Yan et al., In situ exfoliated, edge-rich, oxygen-functionalized graphene from carbon fibers for oxygen electrocatalysis. Adv. Mater. **29**, 1606207 (2017). https://doi.org/10.1002/adma.201606207

185. J. Yu, Y. Dai, Z. Zhang, T. Liu, S. Zhao et al., New nitrogen-doped graphitic carbon nanosheets with rich structural defects and hierarchical nanopores as efficient metal-free electrocatalysts for oxygen reduction reaction in Zn–air batteries. Chem. Eng. Sci. **259**, 117816 (2022). https://doi.org/10.1016/j.ces.2022.117816

186. X.-T. Wang, T. Ouyang, L. Wang, J.-H. Zhong, T. Ma et al., Redox-inert Fe^{3+} ions in octahedral sites of Co–Fe spinel oxides with enhanced oxygen catalytic activity for rechargeable zinc–air batteries. Angew. Chem. Int. Ed. **58**, 13291–13296 (2019). https://doi.org/10.1002/anie.201907595

187. D. Ji, L. Fan, L. Tao, Y. Sun, M. Li et al., The kirkendall effect for engineering oxygen vacancy of hollow Co_3O_4 nanoparticles toward high-performance portable zinc-air batteries. Angew. Chem. Int. Ed. **58**, 13840–13844 (2019). https://doi.org/10.1002/anie.201908736

188. X. Feng, Q. Jiao, H. Cui, M. Yin, Q. Li et al., One-pot synthesis of $NiCo_2S_4$ hollow spheres via sequential ion-exchange as an enhanced oxygen bifunctional electrocatalyst in alkaline solution. ACS Appl. Mater. Interfaces **10**, 29521–29531 (2018). https://doi.org/10.1021/acsami.8b08547

189. Y. Li, J. Yin, L. An, M. Lu, K. Sun et al., Metallic $CuCo_2S_4$ nanosheets of atomic thickness as efficient bifunctional electrocatalysts for portable, flexible Zn–air batteries. Nanoscale **10**, 6581–6588 (2018). https://doi.org/10.1039/c8nr01381k

190. Y. Li, Y. Liu, Q. Qian, G. Wang, G. Zhang, Supramolecular assisted one-pot synthesis of donut-shaped CoP@PNC hybrid nanostructures as multifunctional electrocatalysts for rechargeable Zn–air batteries and self-powered hydrogen production. Energy Storage Mater. **28**, 27–36 (2020). https://doi.org/10.1016/j.ensm.2020.02.022

191. L. Song, T. Zheng, L. Zheng, B. Lu, H. Chen et al., Cobalt-doped basic iron phosphate as bifunctional electrocatalyst for long-life and high-power-density rechargeable zinc–air batteries. Appl. Catal. B Environ. **300**, 120712 (2022). https://doi.org/10.1016/j.apcatb.2021.120712

192. Y.-P. Deng, Y. Jiang, R. Liang, S.-J. Zhang, D. Luo et al., Dynamic electrocatalyst with current-driven oxyhydroxide shell for rechargeable zinc–air battery. Nat. Commun. **11**, 1952 (2020). https://doi.org/10.1038/s41467-020-15853-1

193. K. Ding, J. Hu, W. Jin, L. Zhao, Y. Liu et al., Dianion induced electron delocalization of trifunctional electrocatalysts for rechargeable Zn–air batteries and self-powered water splitting. Adv. Funct. Mater. **32**, 2201944 (2022). https://doi.org/10.1002/adfm.202201944

194. Q. Lai, J. Zhu, Y. Zhao, Y. Liang, J. He et al., MOF-based metal-doping-induced synthesis of hierarchical porous Cu–N/C oxygen reduction electrocatalysts for Zn–air batteries. Small (2017). https://doi.org/10.1002/smll.201700740

195. H.-J. Qiu, P. Du, K. Hu, J. Gao, H. Li et al., Metal and non-metal Co-doped 3D nanoporous graphene for efficient bifunctional electrocatalysis and rechargeable Zn–air batteries. Adv. Mater. **31**, e1900843 (2019). https://doi.org/10.1002/adma.201900843

196. Z. Deng, Q. Yi, G. Li, Y. Chen, X. Yang et al., NiCo-doped C–N nano-composites for cathodic catalysts of Zn-air batteries in neutral media. Electrochim. Acta **279**, 1–9 (2018). https://doi.org/10.1016/j.electacta.2018.05.069

197. J. Qian, X. Guo, T. Wang, P. Liu, H. Zhang et al., Bifunctional porous Co-doped NiO nanoflowers electrocatalysts for rechargeable zinc–air batteries. Appl. Catal. B Environ. **250**, 71–77 (2019). https://doi.org/10.1016/j.apcatb.2019.03.021

198. H. Chang, Y.-F. Guo, X. Liu, P.-F. Wang, Y. Xie et al., Dual MOF-derived Fe/N/P-tridoped carbon nanotube as high-performance oxygen reduction catalysts for zinc-air batteries. Appl. Catal. B Environ. **327**, 122469 (2023). https://doi.org/10.1016/j.apcatb.2023.122469

199. D. Lyu, S. Yao, A. Ali, Z.Q. Tian, P. Tsiakaras et al., N, S Co-doped carbon matrix-encapsulated Co_9S_8 nanoparticles as a highly efficient and durable bifunctional oxygen redox electrocatalyst for rechargeable Zn–air batteries. Adv. Energy Mater. **11**, 2101249 (2021). https://doi.org/10.1002/aenm.202101249

200. B. Qiao, A. Wang, X. Yang, L.F. Allard, Z. Jiang et al., Single-atom catalysis of CO oxidation using Pt_1/FeO_x. Nat. Chem. **3**, 634–641 (2011). https://doi.org/10.1038/nchem.1095

201. P. Rao, D. Wu, T.-J. Wang, J. Li, P. Deng et al., Single atomic cobalt electrocatalyst for efficient oxygen reduction reaction. eScience **2**, 399–404 (2022). https://doi.org/10.1016/j.esci.2022.05.004

202. L. Yang, L. Shi, D. Wang, Y. Lv, D. Cao, Single-atom cobalt electrocatalysts for foldable solid-state Zn–air battery. Nano Energy **50**, 691–698 (2018). https://doi.org/10.1016/j.nanoen.2018.06.023

203. Y.P. Zhu, C. Guo, Y. Zheng, S.Z. Qiao, Surface and interface engineering of noble-metal-free electrocatalysts for efficient energy conversion processes. Acc. Chem. Res. **50**, 915–923 (2017). https://doi.org/10.1021/acs.accounts.6b00635

204. D. Wang, P. Yang, H. Xu, J. Ma, L. Du et al., The dual-nitrogen-source strategy to modulate a bifunctional hybrid Co/Co–N–C catalyst in the reversible air cathode for Zn–air batteries. J. Power. Sources **485**, 229339 (2021). https://doi.org/10.1016/j.jpowsour.2020.229339

205. Q. Cheng, S. Han, K. Mao, C. Chen, L. Yang et al., Co nanoparticle embedded in atomically-dispersed Co–N–C nanofibers for oxygen reduction with high activity and remarkable durability. Nano Energy **52**, 485–493 (2018). https://doi.org/10.1016/j.nanoen.2018.08.005

206. Y. Chen, R. Gao, S. Ji, H. Li, K. Tang et al., Atomic-level modulation of electronic density at cobalt single-atom sites derived from metal–organic frameworks: enhanced oxygen reduction performance. Angew. Chem. Int. Ed. **60**, 3212–3221 (2021). https://doi.org/10.1002/anie.202012798

207. P. Li, H. Wang, X. Tan, W. Hu, M. Huang et al., Bifunctional electrocatalyst with CoN_3 active sties dispersed on N-doped graphitic carbon nanosheets for ultrastable Zn–air batteries. Appl. Catal. B Environ. **316**, 121674 (2022). https://doi.org/10.1016/j.apcatb.2022.121674

208. J. Li, P. Liu, J. Yan, H. Huang, W. Song, Fully-conjugated covalent organic frameworks with two metal sites for oxygen electrocatalysis and Zn–air battery. Adv. Sci. **10**, e2206165 (2023). https://doi.org/10.1002/advs.202206165

209. C.-X. Zhao, J.-N. Liu, J. Wang, D. Ren, J. Yu et al., A $\Delta E = 0.63$ V bifunctional oxygen electrocatalyst enables high-rate and long-cycling zinc–air batteries. Adv. Mater. **33**, e2008606 (2021). https://doi.org/10.1002/adma.202008606

210. S. Chen, X. Liang, S. Hu, X. Li, G. Zhang et al., Inducing Fe $3d$ electron delocalization and spin-state transition of FeN_4 species boosts oxygen reduction reaction for wearable zinc-air battery. Nano-Micro Lett. **15**, 47 (2023). https://doi.org/10.1007/s40820-023-01014-8

211. L. Zong, K. Fan, W. Wu, L. Cui, L. Zhang et al., Anchoring single copper atoms to microporous carbon spheres as high-performance electrocatalyst for oxygen reduction reaction. Adv. Funct. Mater. **31**, 2104864 (2021). https://doi.org/10.1002/adfm.202104864

212. Q. Zhou, J. Cai, Z. Zhang, R. Gao, B. Chen et al., A gas-phase migration strategy to synthesize atomically dispersed Mn–N–C catalysts for Zn–air batteries. Small Methods **5**, e2100024 (2021). https://doi.org/10.1002/smtd.202100024

213. Y. Wang, A. Kumar, M. Ma, Y. Jia, Y. Wang et al., Hierarchical peony-like FeCo–NC with conductive network and highly active sites as efficient electrocatalyst for rechargeable Zn–air battery. Nano Res. **13**, 1090–1099 (2020). https://doi.org/10.1007/s12274-020-2751-7

214. J. Chen, H. Li, C. Fan, Q. Meng, Y. Tang et al., Dual single-atomic Ni–N_4 and Fe–N_4 sites constructing Janus hollow graphene for selective oxygen electrocatalysis. Adv. Mater. **32**, e2003134 (2020). https://doi.org/10.1002/adma.202003134

215. Y. Wang, J. Wu, S. Tang, J. Yang, C. Ye et al., Synergistic Fe–Se atom pairs as bifunctional oxygen electrocatalysts boost

low-temperature rechargeable Zn–air battery. Angew. Chem. Int. Ed. **62**, e202219191 (2023). https://doi.org/10.1002/anie.202219191

216. S. Chandrasekaran, R. Hu, L. Yao, L. Sui, Y. Liu et al., Mutual self-regulation of d-electrons of single atoms and adjacent nanoparticles for bifunctional oxygen electrocatalysis and rechargeable zinc-air batteries. Nano-Micro Lett. **15**, 48 (2023). https://doi.org/10.1007/s40820-023-01022-8

217. C. Huang, Y. Zhang, X. Li, H. Cao, Y. Guo et al., Mn-incorporated Co_3O_4 bifunctional electrocatalysts for zinc–air battery application: an experimental and DFT study. Appl. Catal. B Environ. **319**, 121909 (2022). https://doi.org/10.1016/j.apcatb.2022.121909

218. J. Fu, R. Liang, G. Liu, A. Yu, Z. Bai et al., Recent progress in electrically rechargeable zinc-air batteries. Adv. Mater. **31**, e1805230 (2019). https://doi.org/10.1002/adma.201805230

219. Z. Li, L.E.K. Achenie, H. Xin, An adaptive machine learning strategy for accelerating discovery of perovskite electrocatalysts. ACS Catal. **10**, 4377–4384 (2020). https://doi.org/10.1021/acscatal.9b05248

220. X. Liu, Y. Zhang, W. Wang, Y. Chen, W. Xiao et al., Transition metal and N doping on AlP monolayers for bifunctional oxygen electrocatalysts: density functional theory study assisted by machine learning description. ACS Appl. Mater. Interfaces **14**, 1249–1259 (2022). https://doi.org/10.1021/acsami.1c22309

221. K.V. Graae, P. Norby, Time- and space-resolved in situ X-ray diffraction study of phase transformations and redistribution in Zn–air battery anodes. ACS Appl. Energy Mater. **5**, 11392–11401 (2022). https://doi.org/10.1021/acsaem.2c01868

222. W. Tang, J. Tang, K. Liao, Shao Self-reconstruction of highly active $NiCo_2O_4$ with triple-continuous transfer of electrons, ions, and oxygen for Zn–air batteries. Chem. Eng. J. **455**, 140855 (2023). https://doi.org/10.1016/j.cej.2022.140855

223. Y. Liu, Z. Chen, Z. Li, N. Zhao, Y. Xie et al., CoNi nanoalloy-Co-N_4 composite active sites embedded in hierarchical porous carbon as bi-functional catalysts for flexible Zn–air battery. Nano Energy **99**, 107325 (2022). https://doi.org/10.1016/j.nanoen.2022.107325

224. L. Yang, D. Wang, Y. Lv, D. Cao, Nitrogen-doped graphitic carbons with encapsulated CoNi bimetallic nanoparticles as bifunctional electrocatalysts for rechargeable Zn–Air batteries. Carbon **144**, 8–14 (2019). https://doi.org/10.1016/j.carbon.2018.12.008

225. Y. Zhang, Z. Zhang, G. Jiang, A.H. Mamaghani, S. Sy et al., Three-dimensionally ordered mesoporous Co_3O_4 decorated with Mg as bifunctional oxygen electrocatalysts for high-performance zinc–air batteries. Nano Energy **100**, 107425 (2022). https://doi.org/10.1016/j.nanoen.2022.107425

226. X. Zheng, Y. Cao, Z. Wu, W. Ding, T. Xue et al., Rational design and spontaneous sulfurization of NiCo-(oxy)hydroxysulfides nanosheets with modulated local electronic configuration for enhancing oxygen electrocatalysis. Adv. Energy Mater. **12**, 2103275 (2022). https://doi.org/10.1002/aenm.202103275

227. H.S. Leipner, C.G. Hübner, T.E.M. Staab, M. Haugk, R. Krause-Rehberg, Positron annihilation at dislocations and related point defects in semiconductors. Phys. Stat. Sol. (A) **171**, 377–382 (1999). https://doi.org/10.1002/(SICI)1521-396X(199901)171:1%3C377::AID-PSSA377%3E3.0.CO;2-A

228. S. Ghosh, G.G. Khan, K. Mandal, A. Samanta, P.M.G. Nambissan, Evolution of vacancy-type defects, phase transition, and intrinsic ferromagnetism during annealing of nanocrystalline TiO_2 studied by positron annihilation spectroscopy. J. Phys. Chem. C **117**, 8458–8467 (2013). https://doi.org/10.1021/jp3115836

229. X. Zheng, Y. Cao, H. Wang, J. Zhang, M. Zhao et al., Designing breathing air-electrode and enhancing the oxygen electrocatalysis by thermoelectric effect for efficient Zn–air batteries. Angew. Chem. Int. Ed. **62**, e202302689 (2023). https://doi.org/10.1002/anie.202302689

230. Z. Sun, H. Zhang, L. Cao, X. Liu, D. Wu et al., Understanding synergistic catalysis on Cu–Se dual atom sites via operando X-ray absorption spectroscopy in oxygen reduction reaction. Angew. Chem. Int. Ed. **62**, e202217719 (2023). https://doi.org/10.1002/anie.202217719

231. Y.-P. Deng, Y. Jiang, R. Liang, N. Chen, W. Chen et al., Reconstructing $3d$-metal electrocatalysts through anionic evolution in zinc-air batteries. J. Am. Chem. Soc. **145**, 20248–20260 (2023). https://doi.org/10.1021/jacs.3c03214